nature

SUPPLEMENTARY INFORMATION

https://doi.org/10.1038/s41586-018-0747-1

In the format provided by the authors and unedited.

Industrial and agricultural ammonia point sources exposed

Martin Van Damme[1,3]*, Lieven Clarisse[1,3]*, Simon Whitburn[1], Juliette Hadji-Lazaro[2], Daniel Hurtmans[1], Cathy Clerbaux[1,2] & Pierre-François Coheur[1]

[1]Université libre de Bruxelles (ULB), Service de Chimie Quantique et Photophysique, Atmospheric Spectroscopy, Brussels, Belgium. [2]LATMOS/IPSL, UPMC Université Paris-06, Sorbonne Universités, UVSQ, CNRS, Paris, France. [3]These authors contributed equally: Martin Van Damme, Lieven Clarisse. *e-mail: martin.van.damme@ulb.ac.be; lclariss@ulb.ac.be

A. Hotspot illustrations: The 28 hotspots indicated in the map below (Figure SI1) were used to illustrate the results of the paper. For each of them, a detailed six-panel figure is provided below. The six panels are respectively:

(a) The nine-year average IASI-NH_3 distribution (0.01°×0.01° high-resolution grid, 10^{16} molecules cm^{-2}, with varying colour scale). The latitude-longitude limits of this subplot correspond to the size of the box considered for the satellite-based flux calculation.
(b) Zoom of the visible imagery map from Google Earth of the assumed NH_3 point source(s). The zoomed area is indicated with a white rectangle in the panel (a).
(c) NH_3 column distribution (in 10^{16} molecules cm^{-2}, note that a fixed colour scale has been used for all the illustrations, allowing comparison) obtained after subtracting the calculated background (10^{th} percentile). The satellite-based flux estimate is provided in the title (kg s^{-1}).
(d) Temporal evolution of the satellite-based emission fluxes (kg s^{-1}).
(e) Industrial and (f) agricultural emissions distributions (10^{-5} kg s^{-1}) from the EDGAR v4.3.1 inventory. The EDGAR flux estimates are provided in the titles (kg s^{-1}).
The black contour in panel (a), (e) and (f) indicates the 90^{th} percentile value from all the 0.01°×0.01° averaged observed columns in the considered box. This area was then used to determine the EDGAR emission fluxes (Methods).

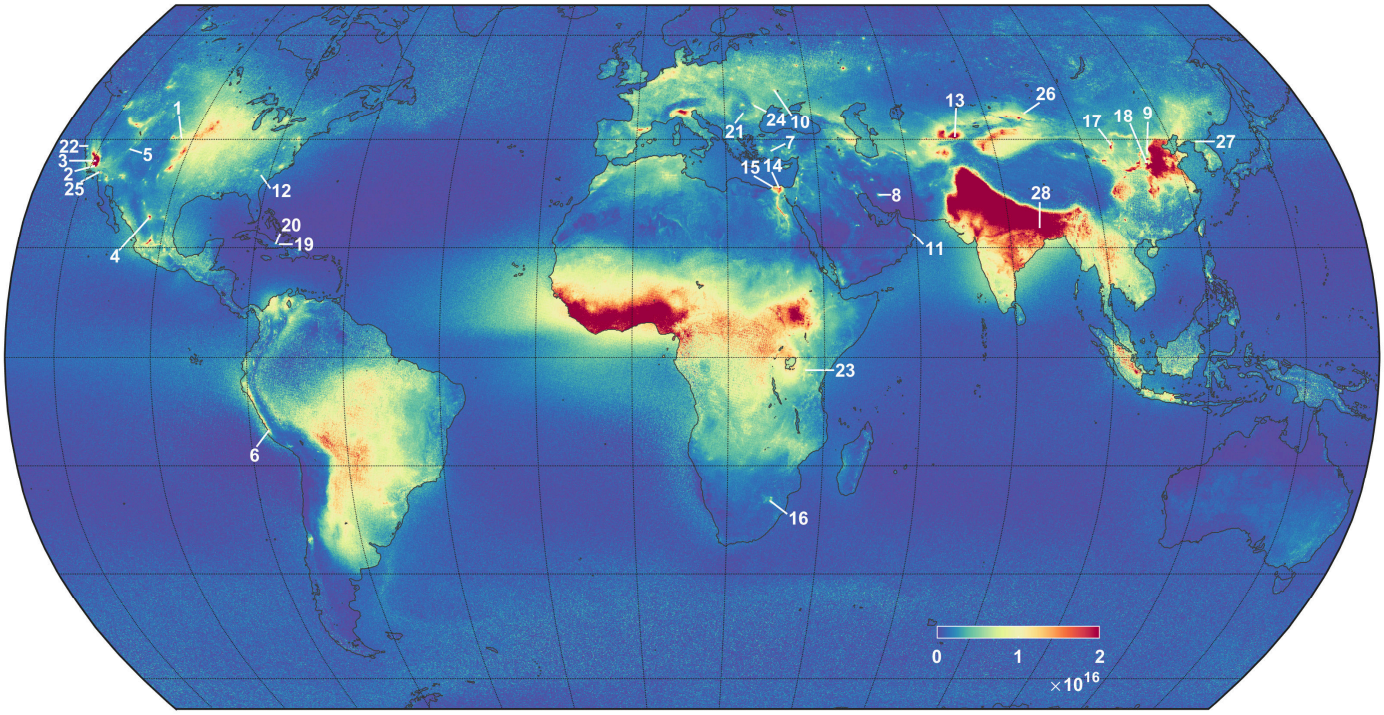

Figure SI1: Location of the hotspots discussed in the main text on top of the global nine-year NH_3 average (molecules cm^{-2}). The different sites are, by order of citation in the text: Eckley – Yuma (1, USA), Backersfield (2, USA), Tulare (3, USA), Torreon (4, Mexico), Milford (5, USA), Alto Laran District (6, Peru), Basmakci (7, Turkey), Marvdasht (8, Iran), Pingsongxiang (9, China), Cherkasy (10, Ukraine), Sur Industrial Estate (11, Oman), Beech Island (12, USA), Ferghana (13, Uzbekistan), Talkha (14, Egypt), Abu Qir (15, Egypt), Secunda (16, South Africa), Shizuishan (17, China), Zezhou – Gaoping (18, China), Moa (19, Cuba), Nicaro (20, Cuba), Stuparei (21, Romania), The Geysers (22, USA), Lake Natron (23, Tanzania), Bacau (24, Romania), Chino (25, USA), Wucaiwan (26, China), Anju (27, North Korea), Jharia (28, India).

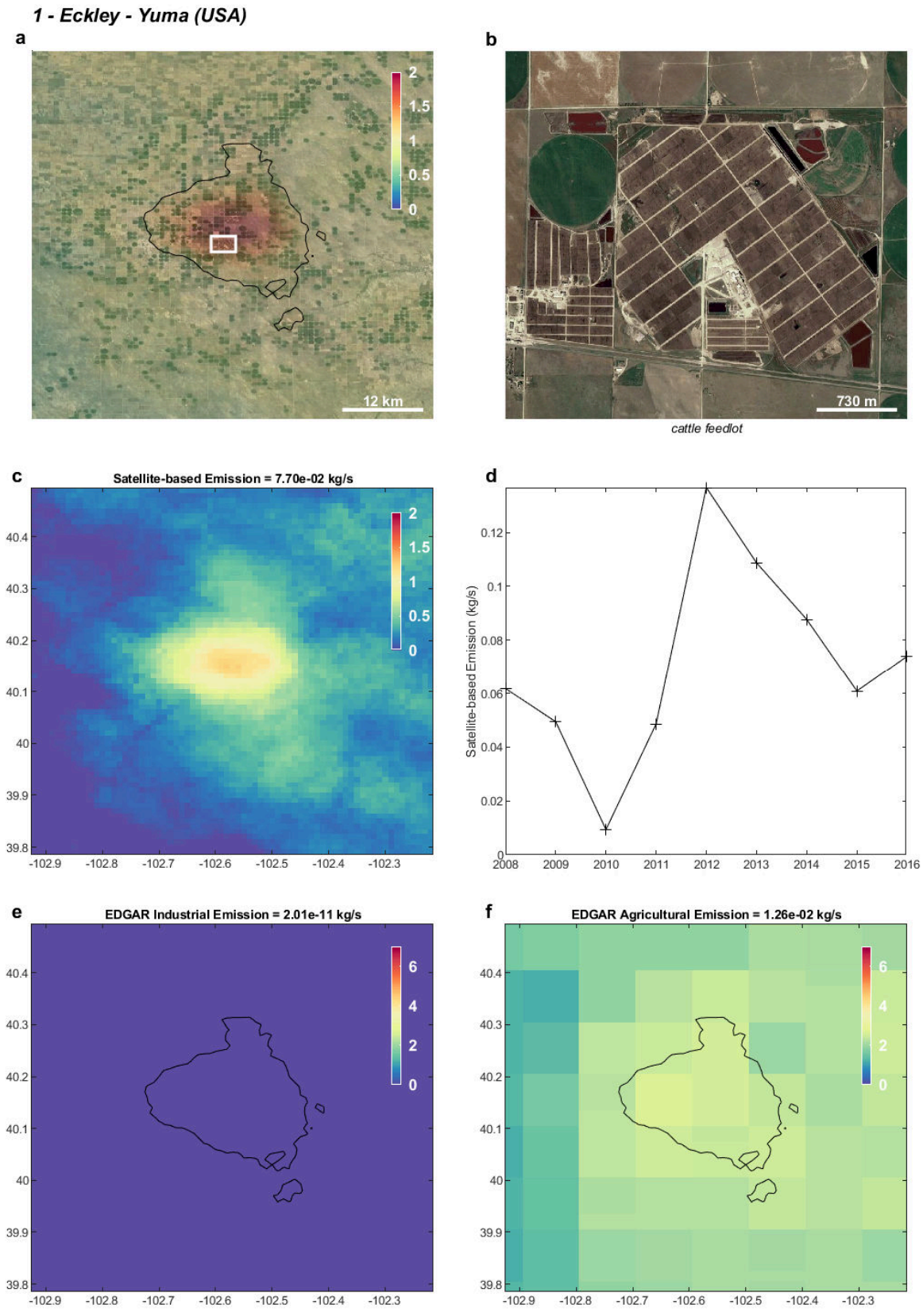

An isolated feedlot with a capacity of over 100,000 head of cattle is seen in Northeast Colorado amid a much larger area of pivot irrigated crop fields. See also Yuan et al. (2017) where emissions from similar “Concentrated animal feeding operations (CAFOs)” in Colorado are discussed[1].

[1] Yuan, B. *et al.* Emissions of volatile organic compounds (VOCs) from concentrated animal feeding operations (CAFOs): chemical compositions and separation of sources. *Atmos. Chem. Phys.* **17**, 4945-4956 (2017).

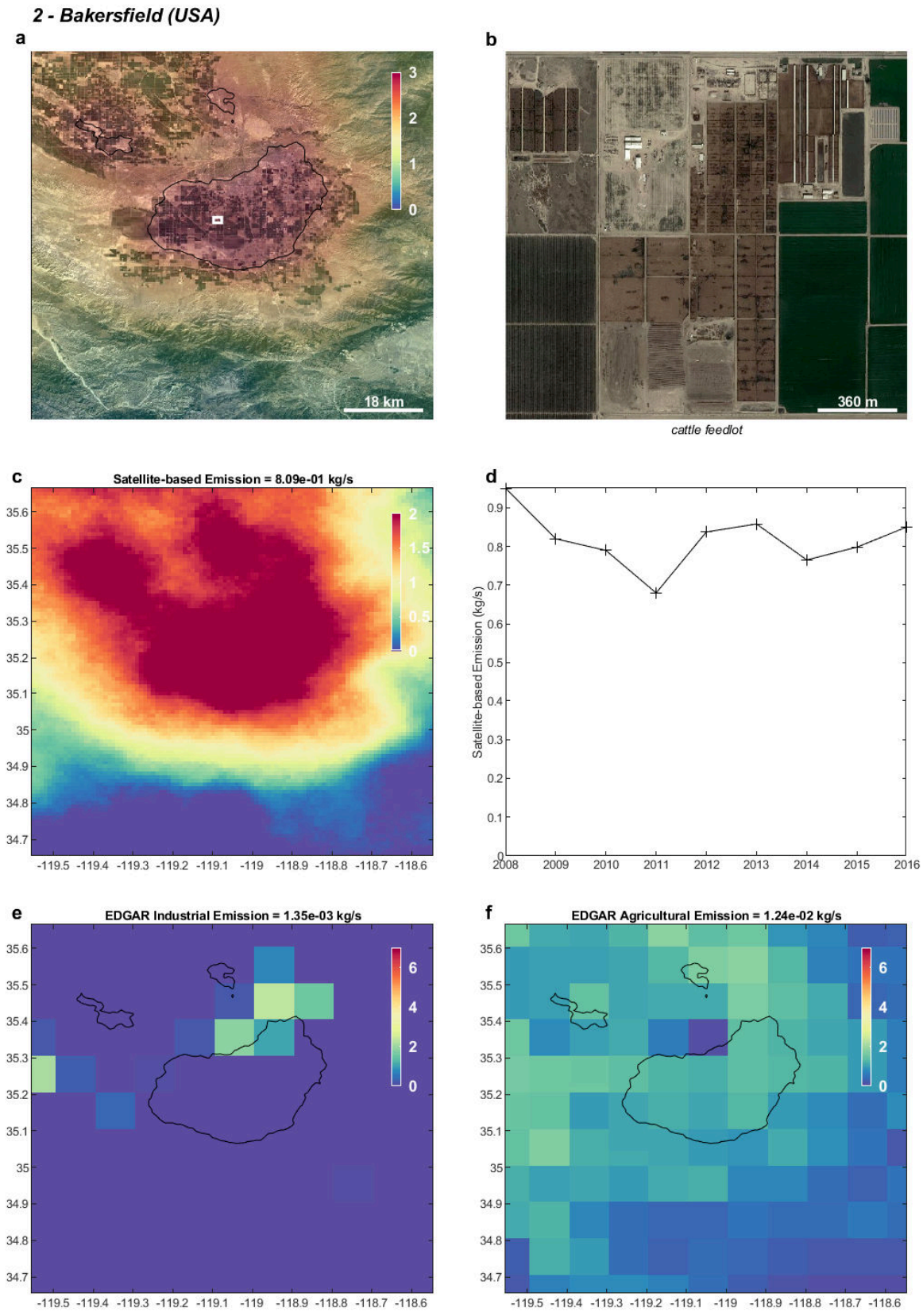

Bakersfield and Tulare (see next page) are the two largest hotspots within the agricultural valley of San Joaquin, California[1]. Both of them are home to many large feedlots. Massive slurry pits can also be spotted adjacent to some of the feedlots.

[1] Clarisse, L. *et al.* Satellite monitoring of ammonia: A case study of the San Joaquin Valley. *J. Geophys. Res.* **115**, D13302 (2010).

3 - Tulare (USA)

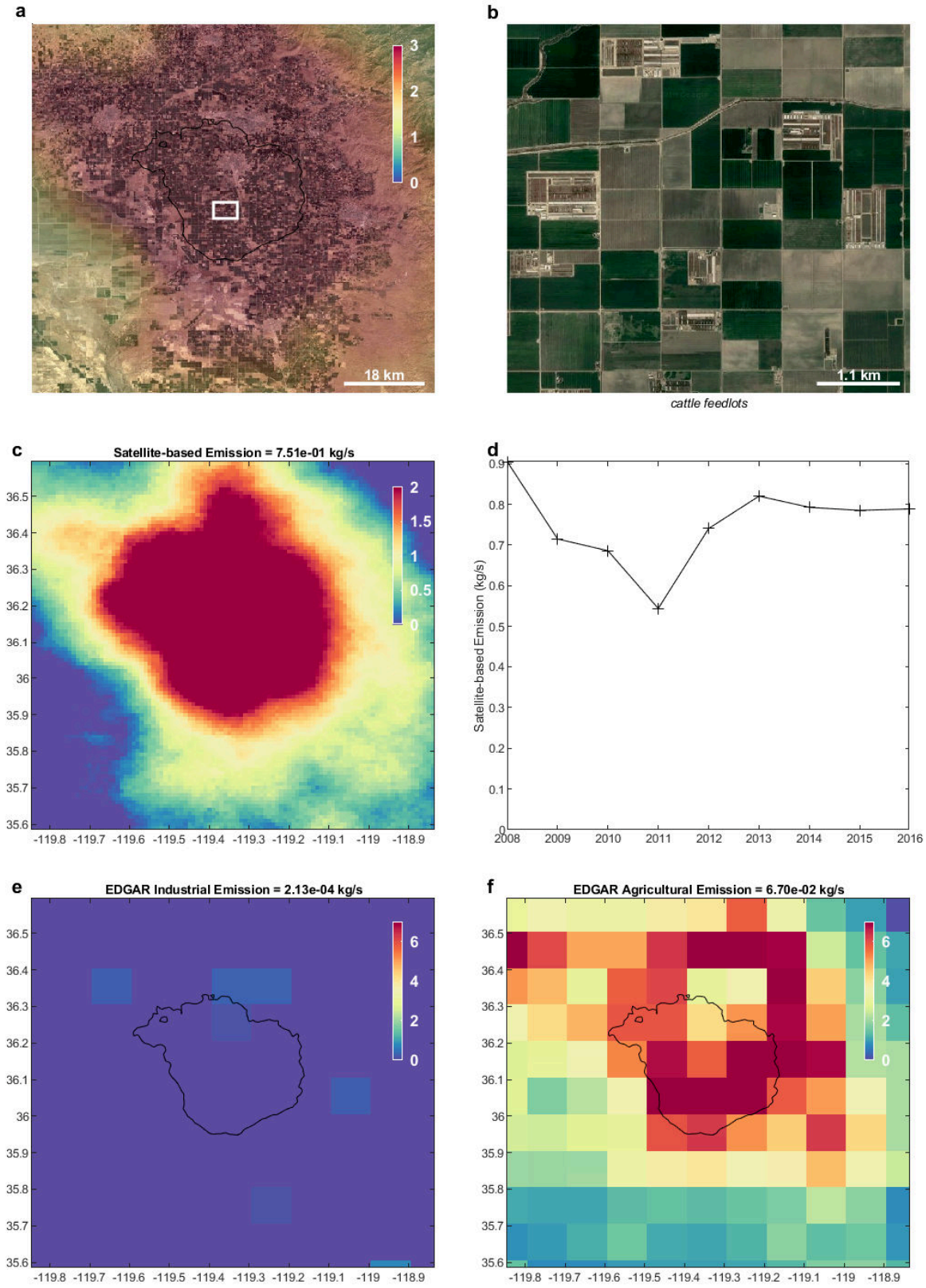

See previous.

4 - Torreon (Mexico)

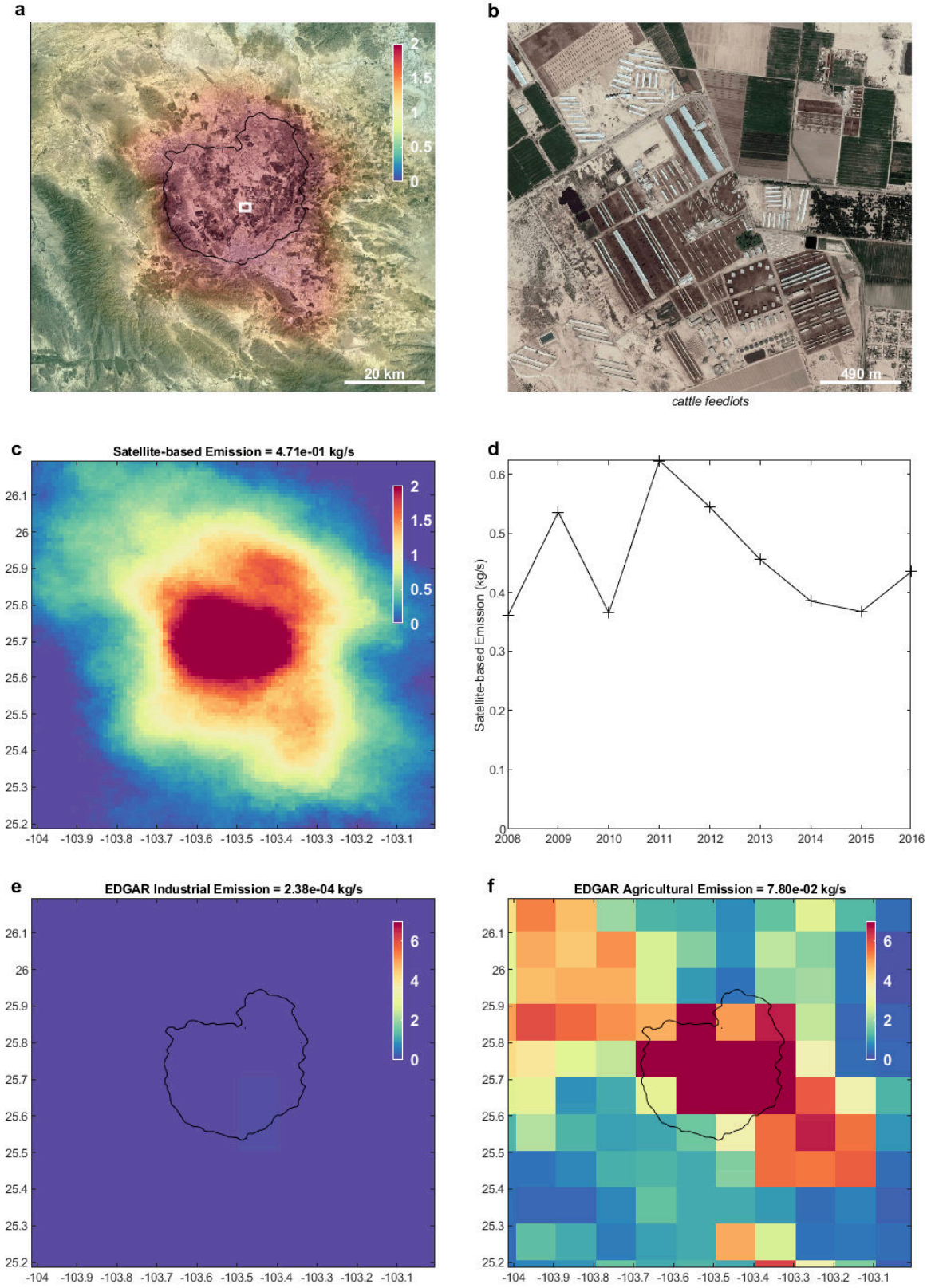

In the 19th century the area was already a centre of animal farming (then appropriately called Torreon Ranch), and it fulfils this role until today. The imagery shows some of the very large feedlots just north of Torreon.

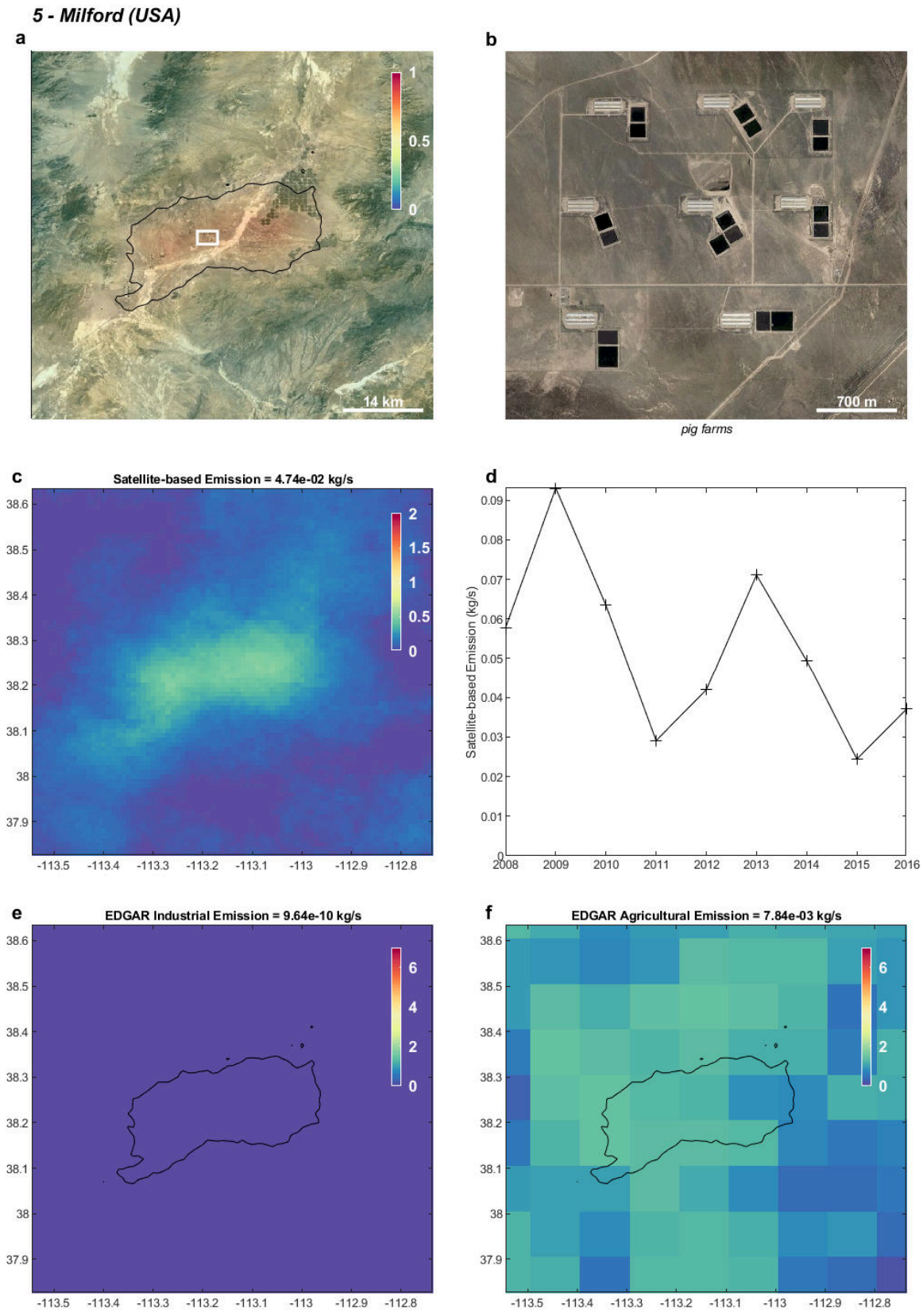

Hog farms with associated slurry pits (also known as slurry lagoons) where animal waste is kept and recycled. Each pit measures some 130×130 m².

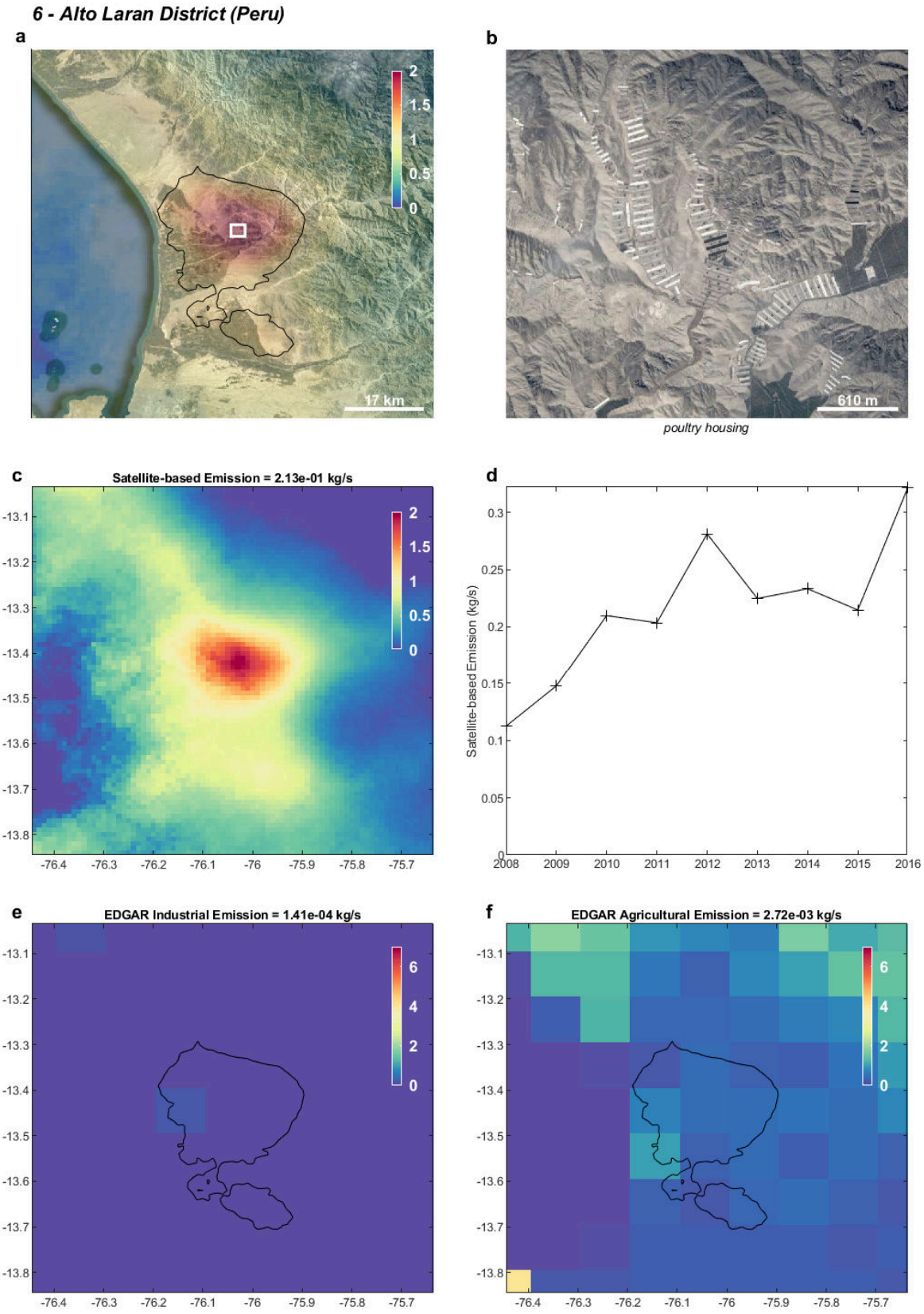

Poultry farms (egg production) on the coast of Peru. A plethora of similar hotspots are found along the coast of Peru, most of which are also related to poultry farming. The trend observed is consistent with reported increased egg production in Peru[1].

[1] FAOSTAT, http://www.fao.org/faostat/en/#home (last accessed 27 April 2018).

7 - Basmakci (Turkey)

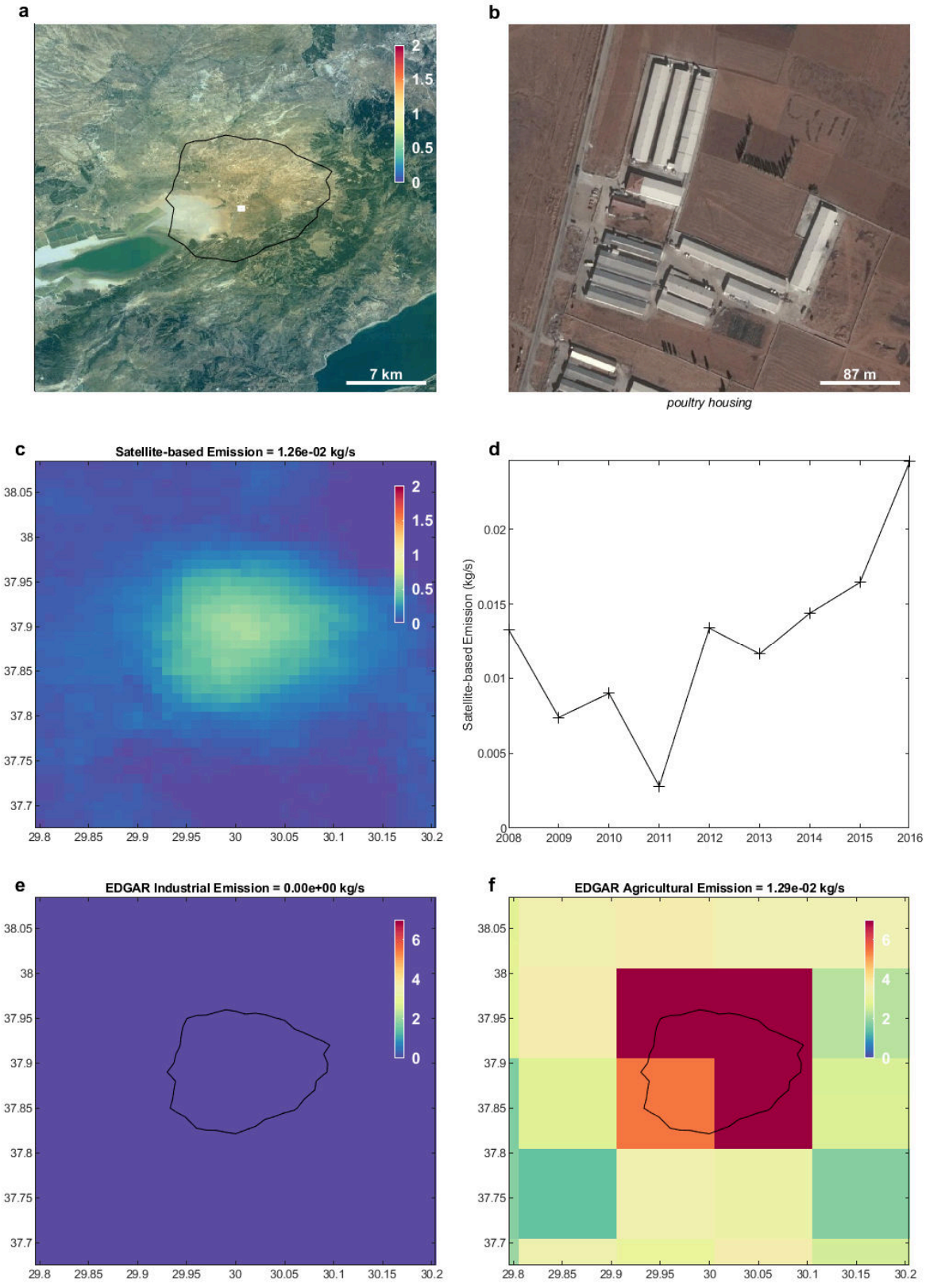

This area accommodates the largest producers of table eggs in Turkey[1]. The NH_3 hotspot is observed slightly west and south of the city, where also the largest livestock housing are seen.

[1] Yasar, S., Orhan, H., & Erensayin, C. Examining the nutritional and production characteristics of egg-farms in Basmakci County in Turkey. *Worlds Poult. Sci. J.* **59**(2), 249-259 (2003).

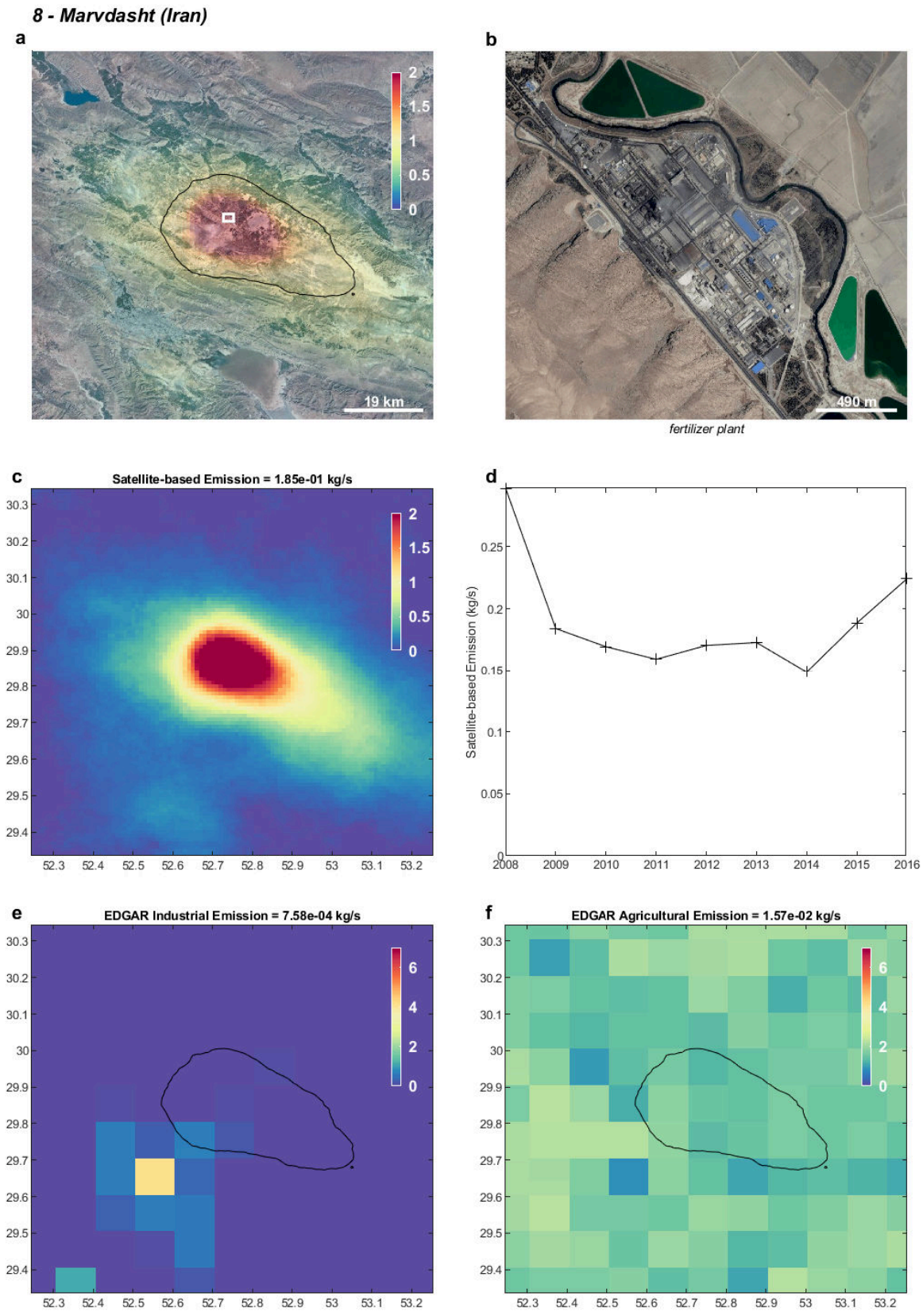

Apart from the Nile river and delta, this is the largest and most pronounced hotspot in the Middle East. It is centred around a petrochemical ammonia plant which was established in 1964, and as of 2016 produces $1.1 \cdot 10^6$ tons of NH_3 per year[1].

[1] IFDC. Worldwide Ammonia Capacity Listing by Plant. Fertilizer Situation Reports (2016). IFDC-FSR-10.

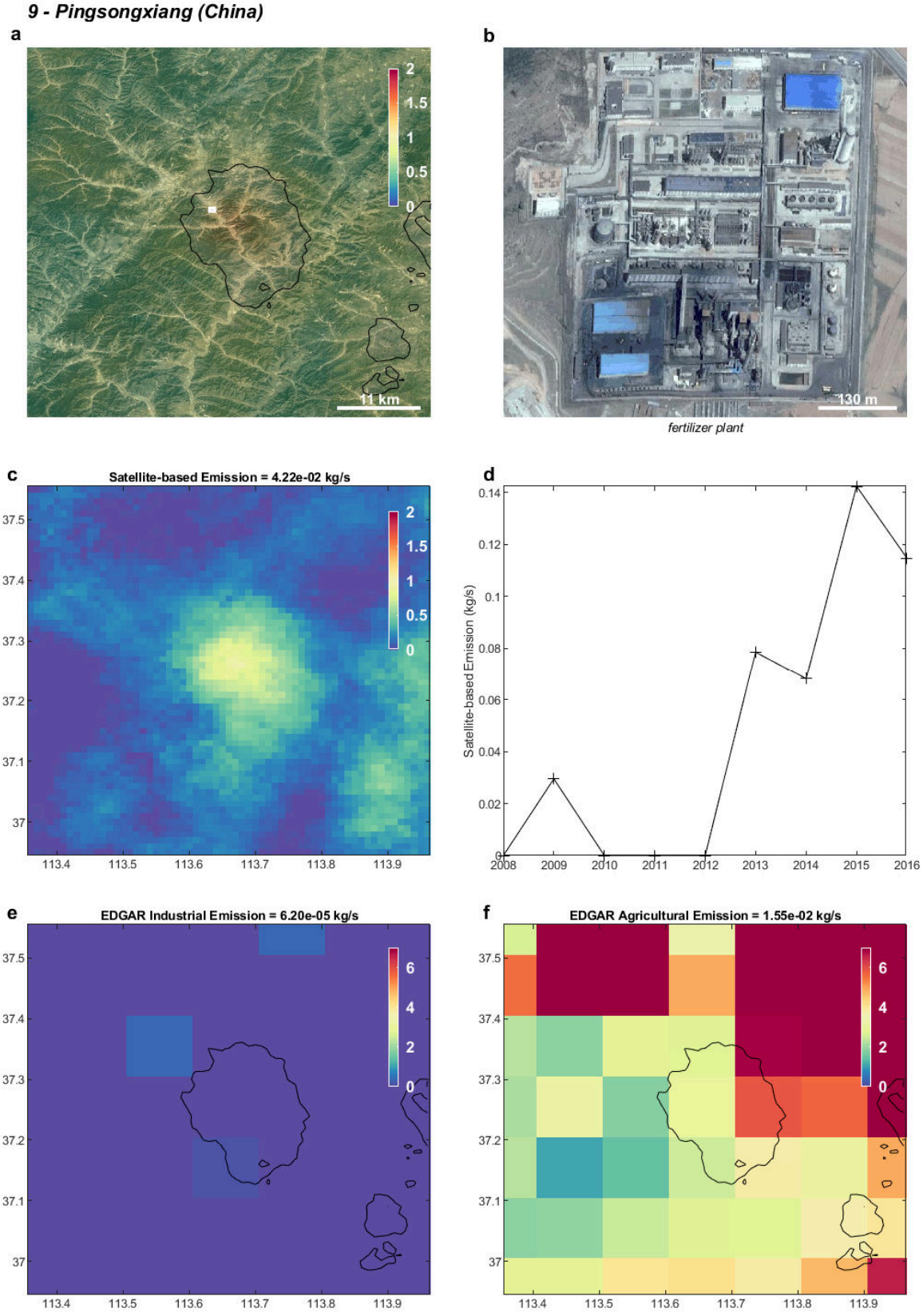

An example of a well-isolated coal-based fertilizer plant (ammonia and urea). It opened in 2009, but NH_3 enhancements are only observed from 2013. The plant is, as far as we know, not included in the IFDC list[1] nor in the SYNGAS database[2].

[1] IFDC. Worldwide Ammonia Capacity Listing by Plant. Fertilizer Situation Reports (2016). IFDC-FSR-10; [2] GSTC. Worldwide syngas database (2018). www.globalsyngas.org (last access: 29/01/2018).

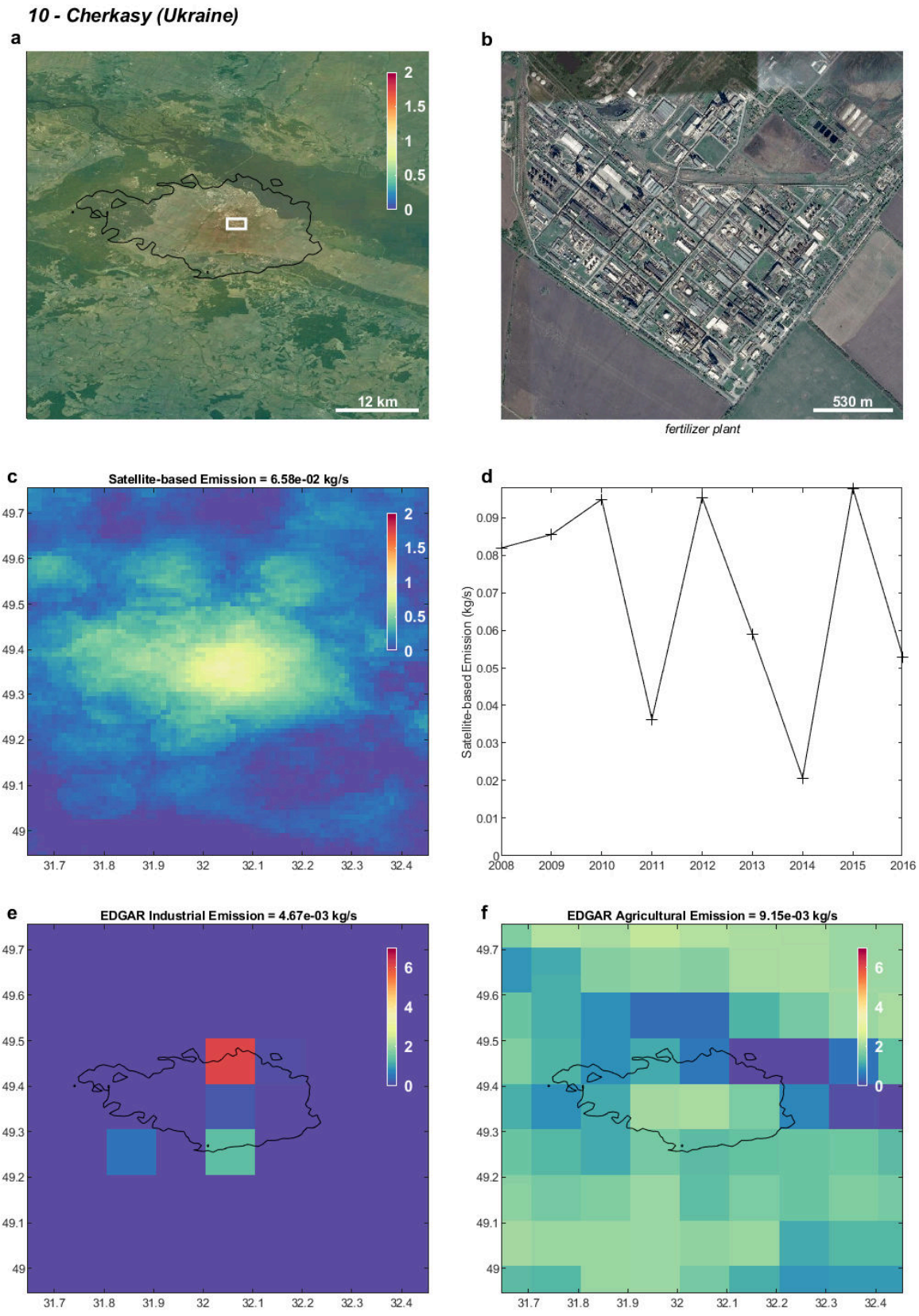

Cherkasy headquarters Ukraine's largest ammonia production plant with a production of $1.4 \cdot 10^6$ metric tons of NH_3 per year[1]. Established in 1965. As testified by newspaper reports, the plant recently underwent repairs and modernisations, and the interruptions of activities can explain what is observed in the time evolution.

[1] IFDC. Worldwide Ammonia Capacity Listing by Plant. Fertilizer Situation Reports (2016). IFDC-FSR-10.

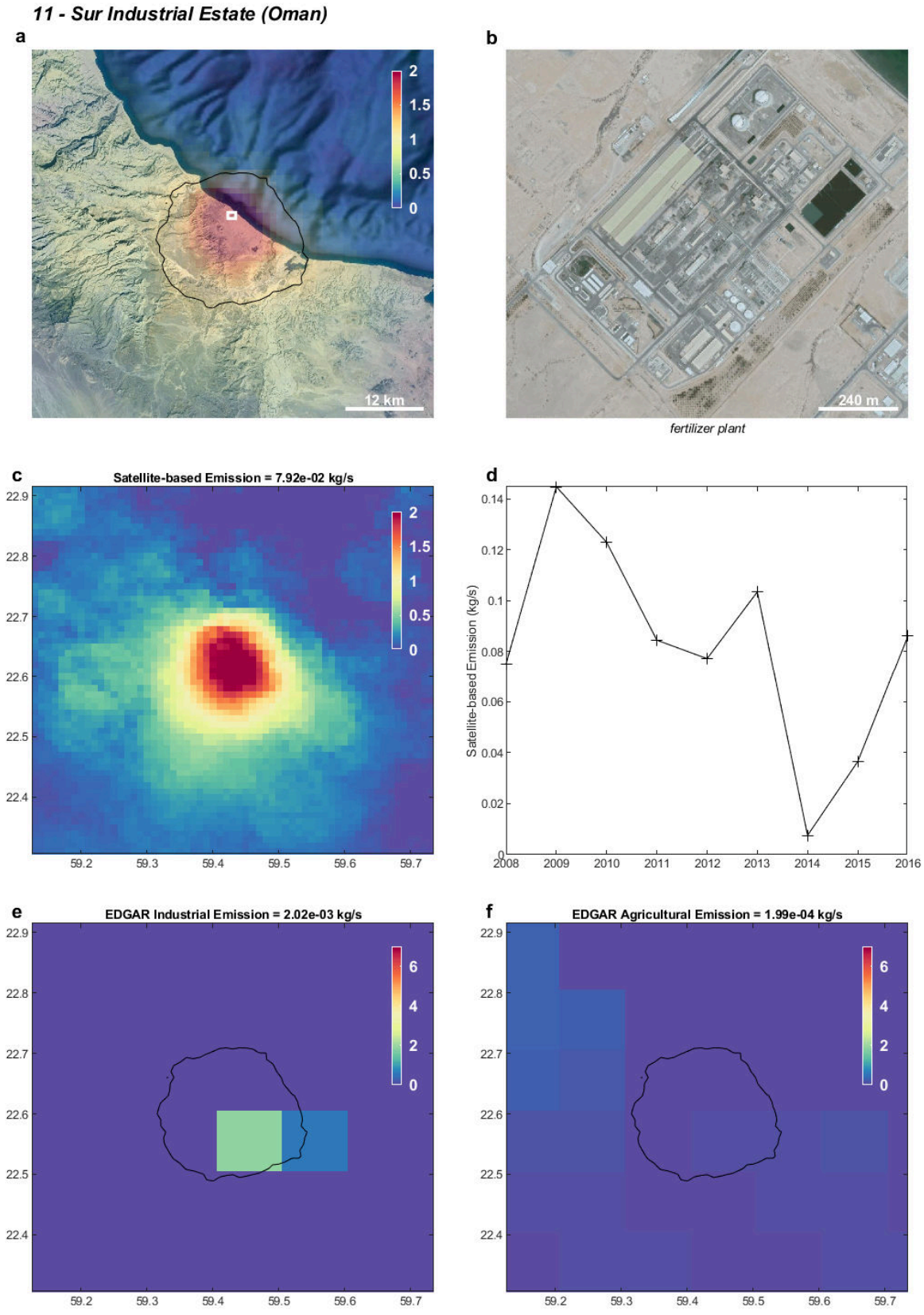

Natural gas-based fertilizer plant (ammonia and urea), which was established in 2005. It is the only NH_3 enhancement observed over Oman.

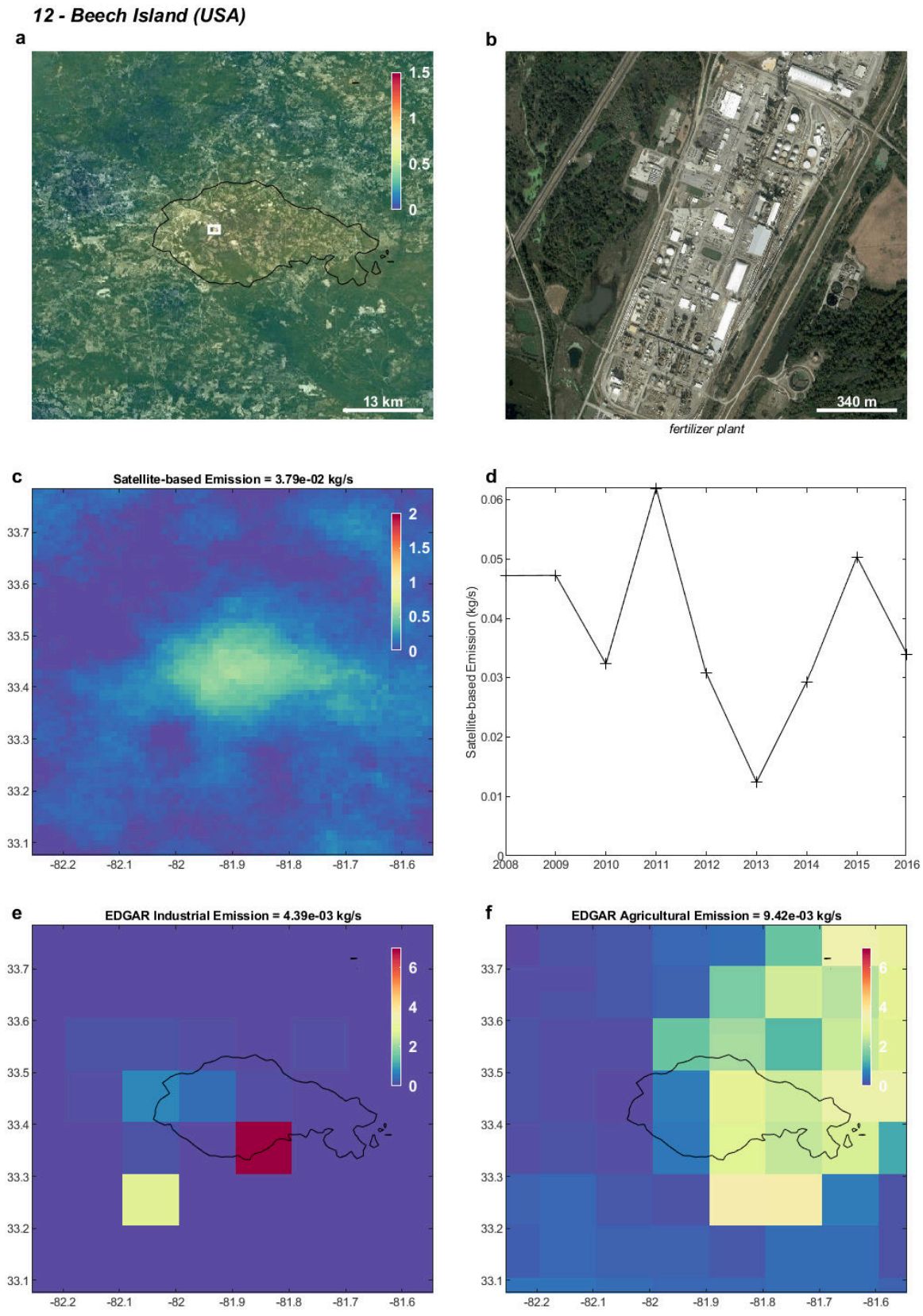

One of the few hotspots in the US (Georgia) related to industrial fertilizer production. Observed columns are however much lower than the emissions of fertilizer industry in e.g. the Middle East, Eastern Europe or Asia.

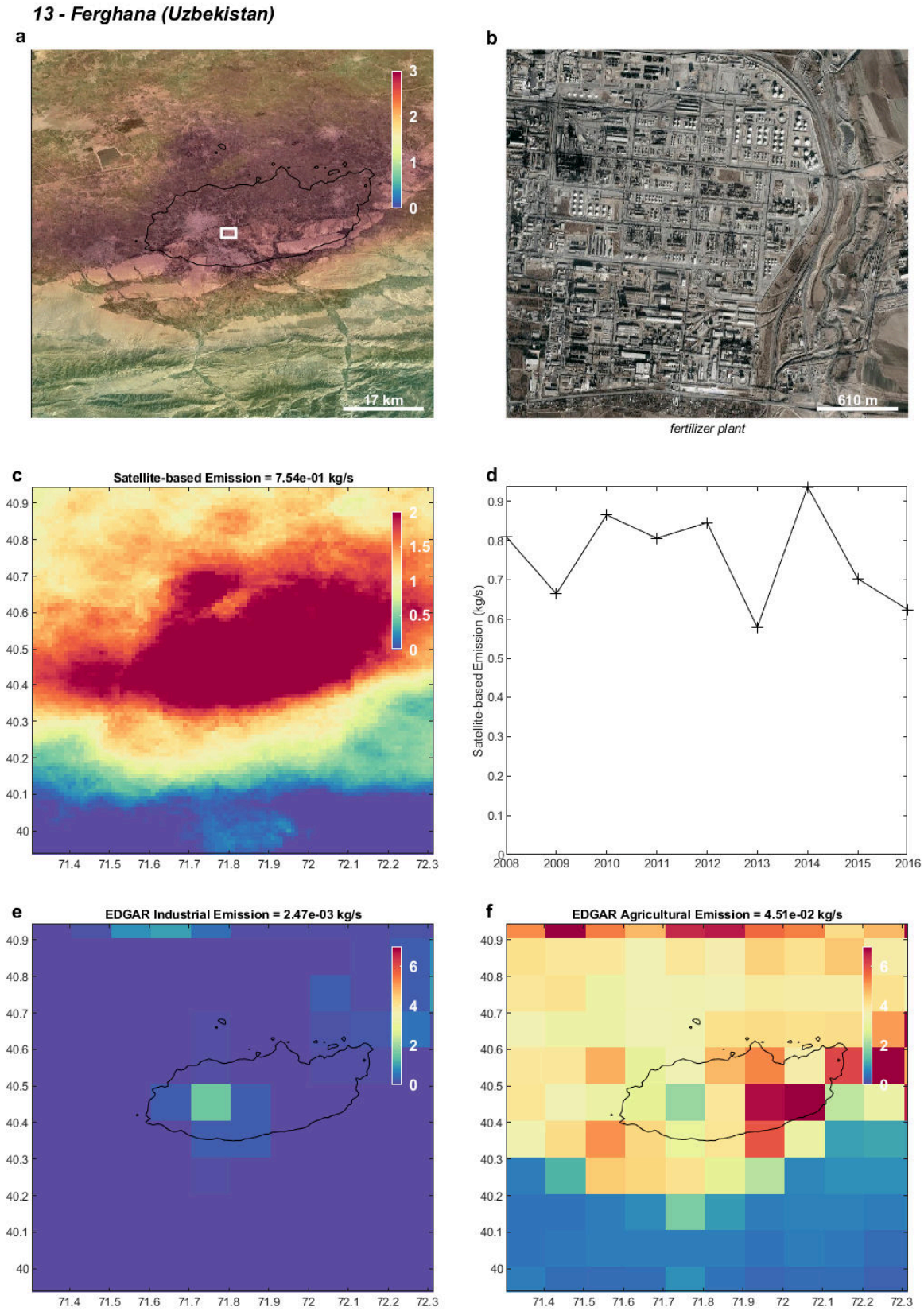

The Ferghana Valley is a region of intense agricultural activity. The south central part of the valley features “a hotspot in a hotspot” (best seen here in panel a), which coincides with the location of an important fertilizer plant.

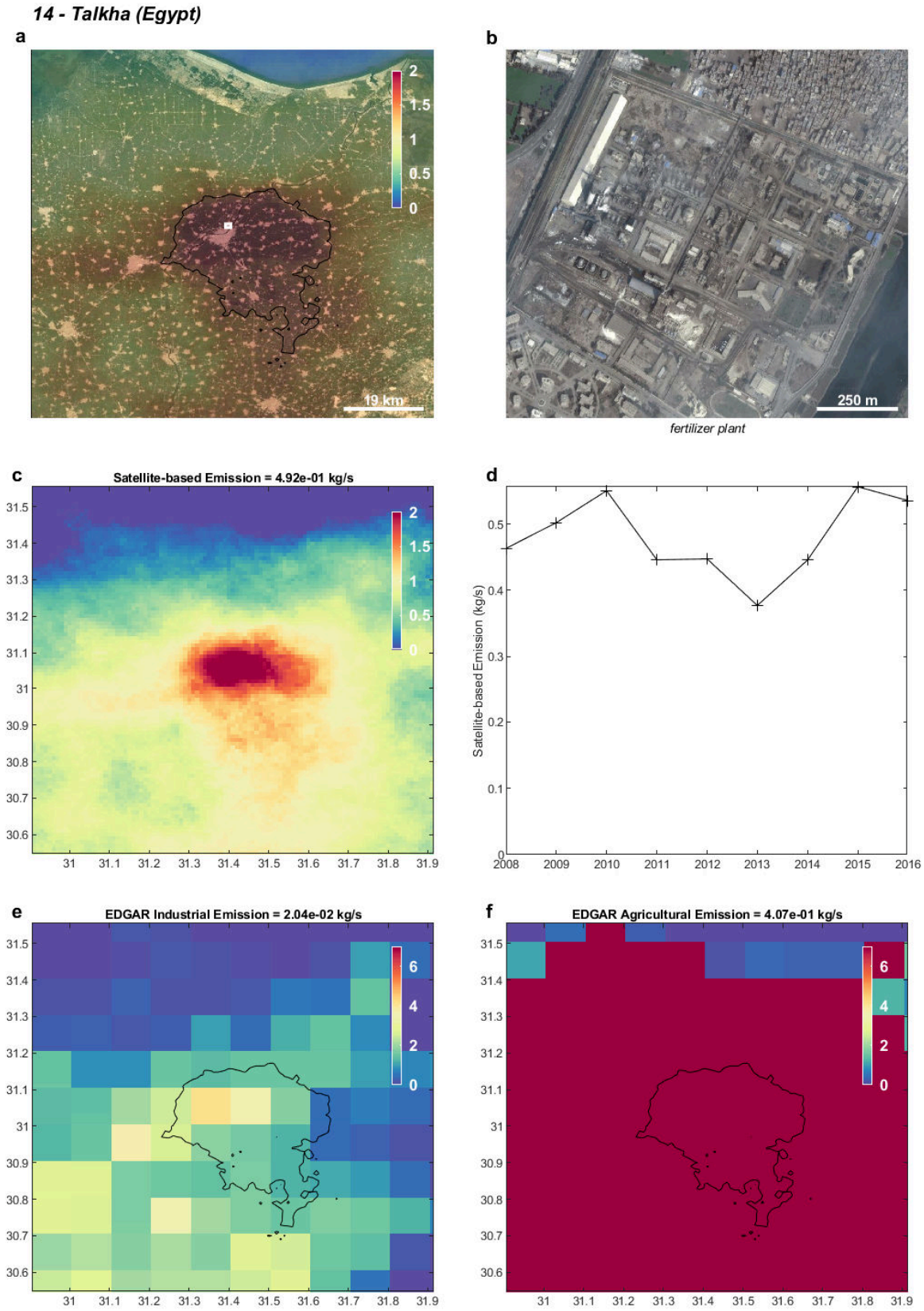

Very much like the fertilizer plant in the Ferghana Valley, the hotspots seen over Talkha and Abu Qir in the Nile Delta are “hotspots in a hotspot”, corresponding to industrial fertilizer production within an intense agricultural area.

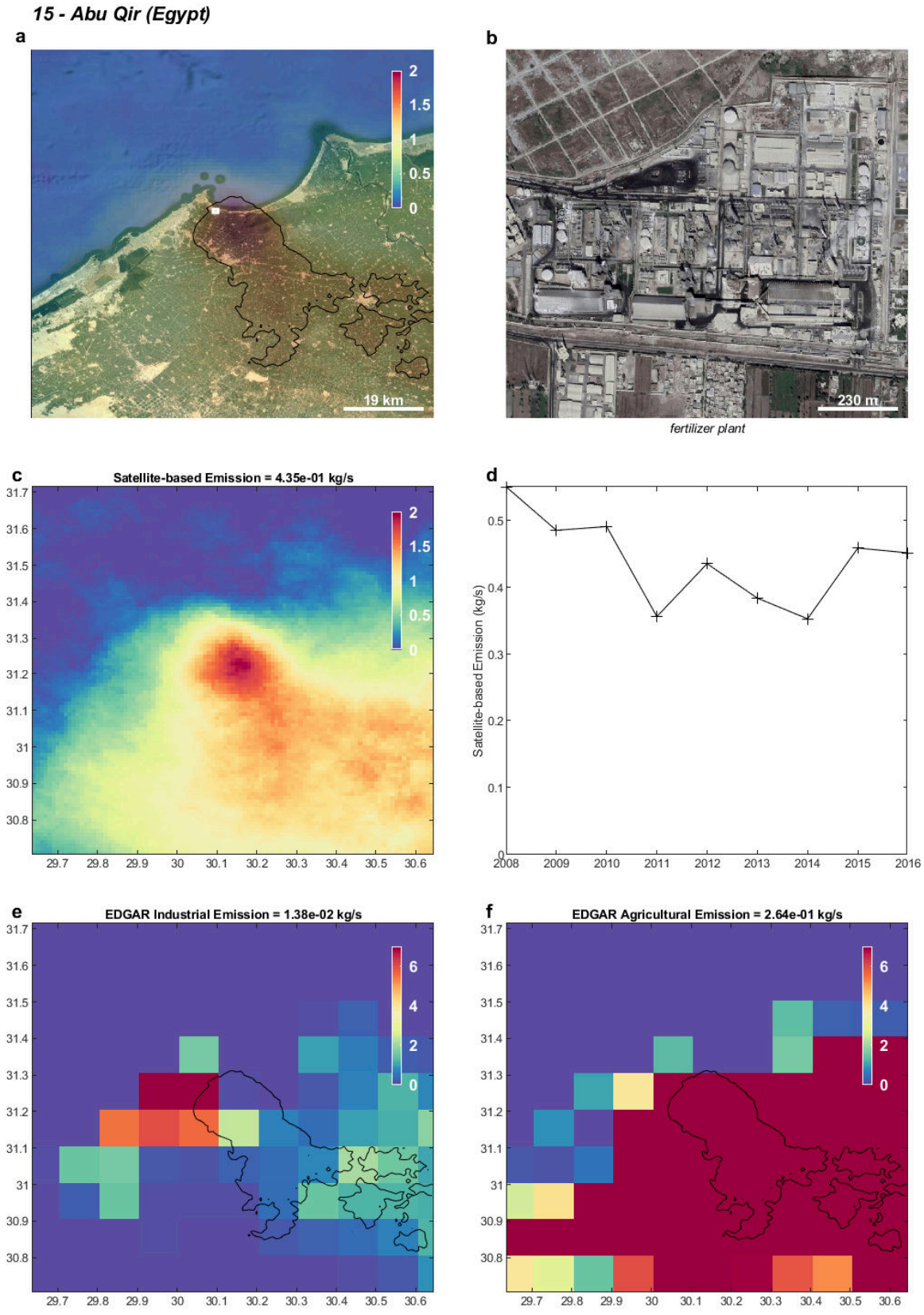

See previous.

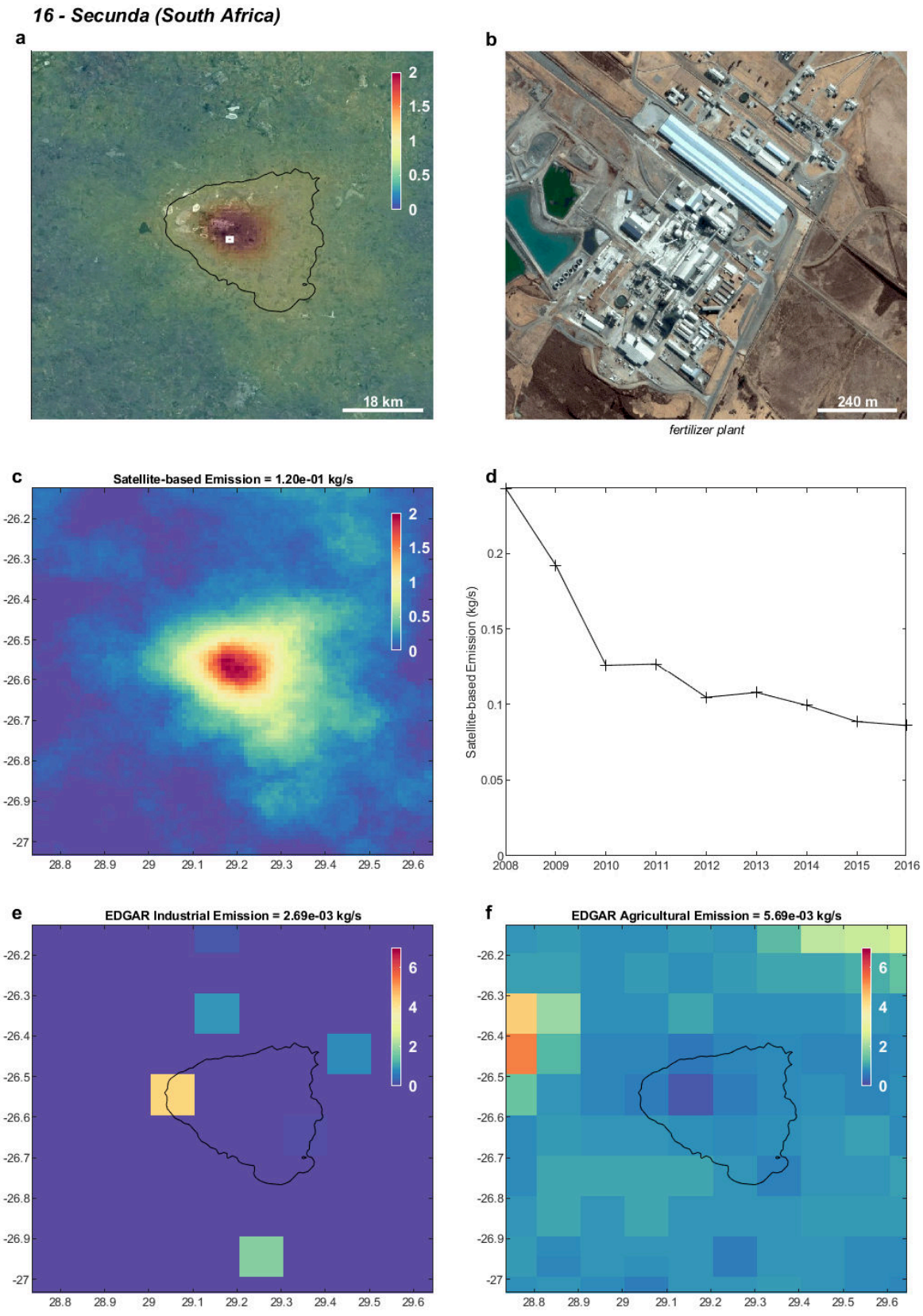

Amid underground coal mines in Secunda lies the largest coal liquefaction plant in the world. The location of its associated fertilizer plant coincides with the centre of the observed NH_3 hotspot.

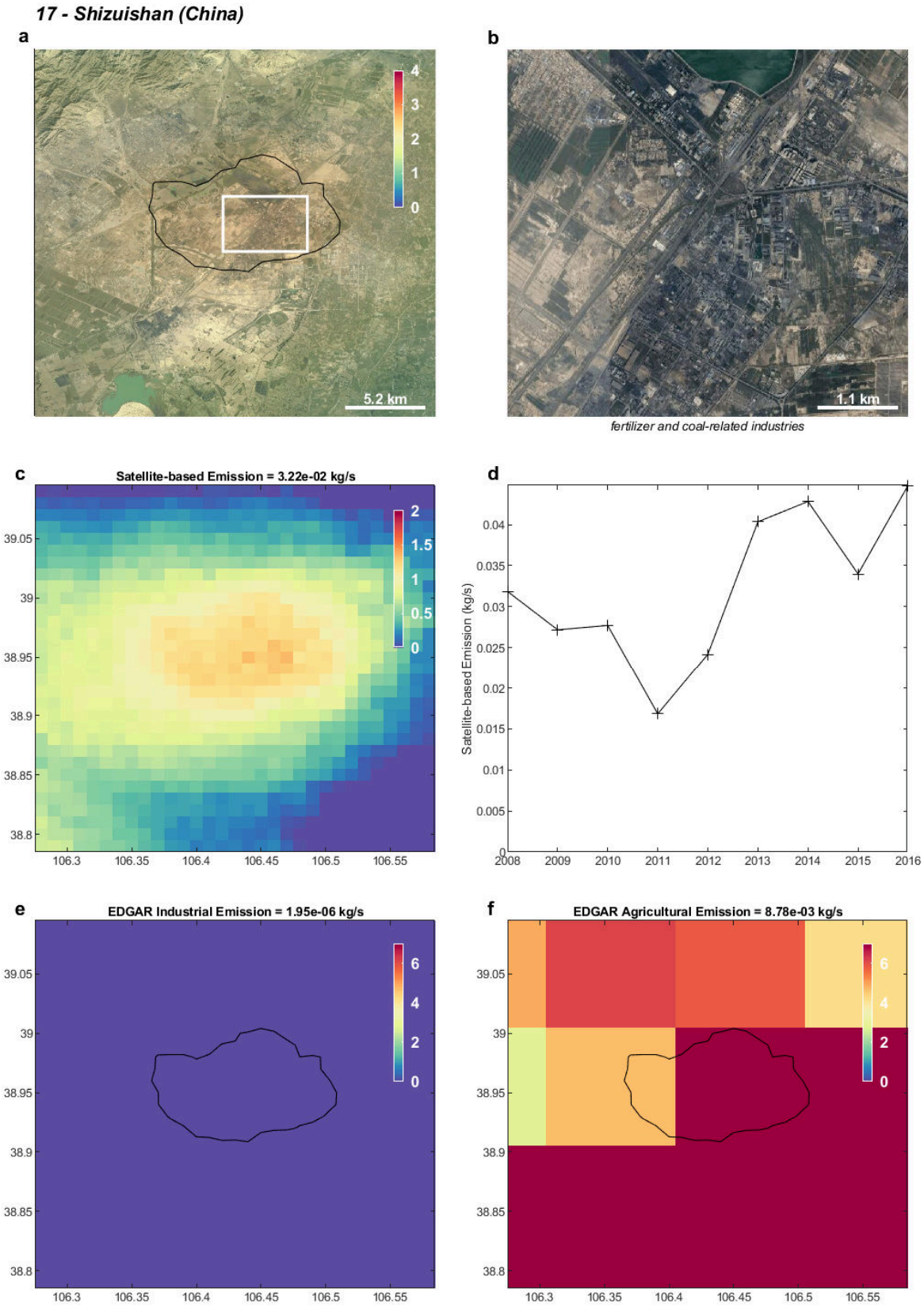

The exact location of the hotspot is near the town Taixi (Pingluo, Shizuishan) in the Ningxia province. It features a large coal-based industrial park, shown in panel b.

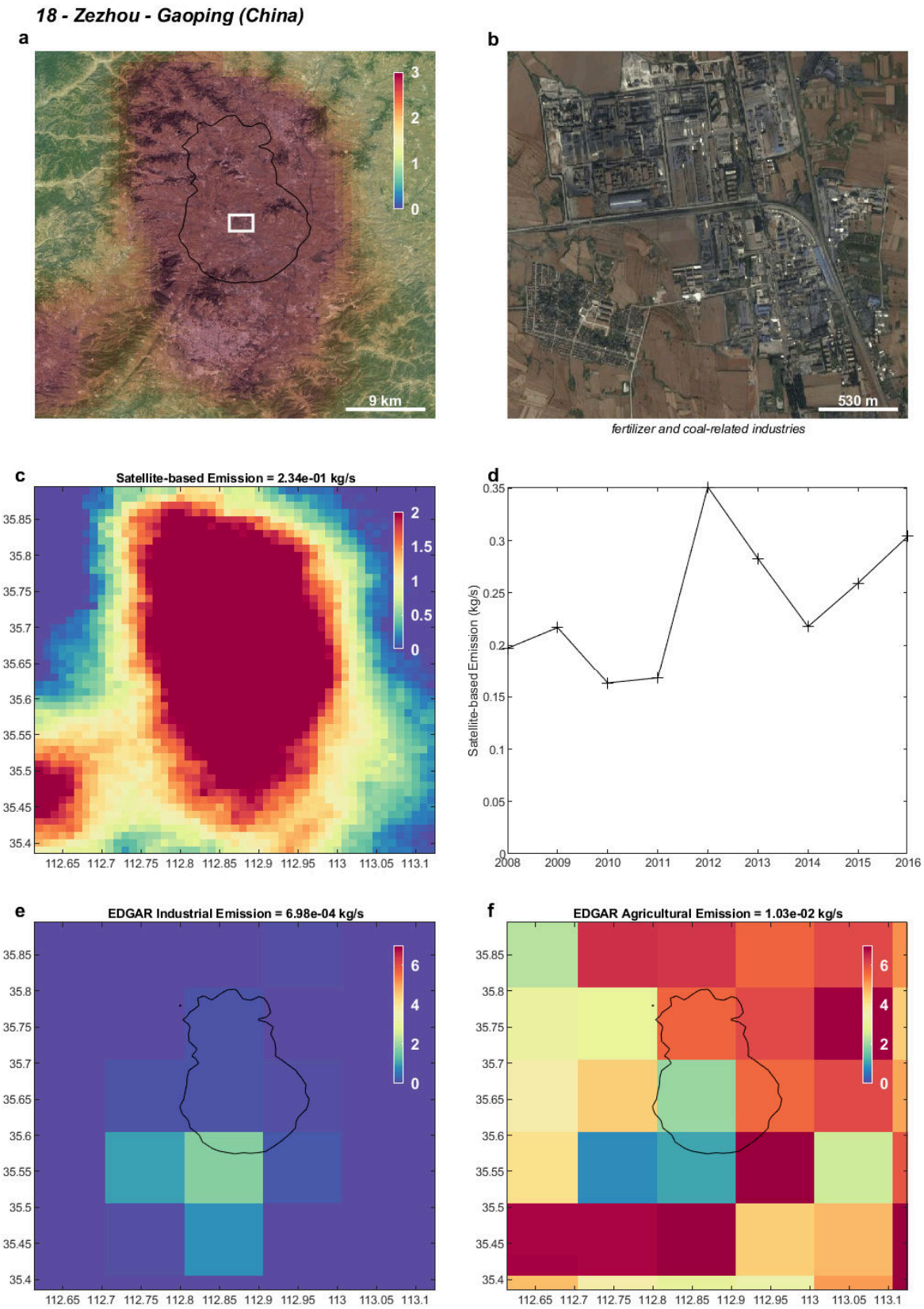

The largest NH_3 columns in China are measured in Zezhou (Shanxi county). The area features several large industrial parks (coal-based industry, including fertilizer production).

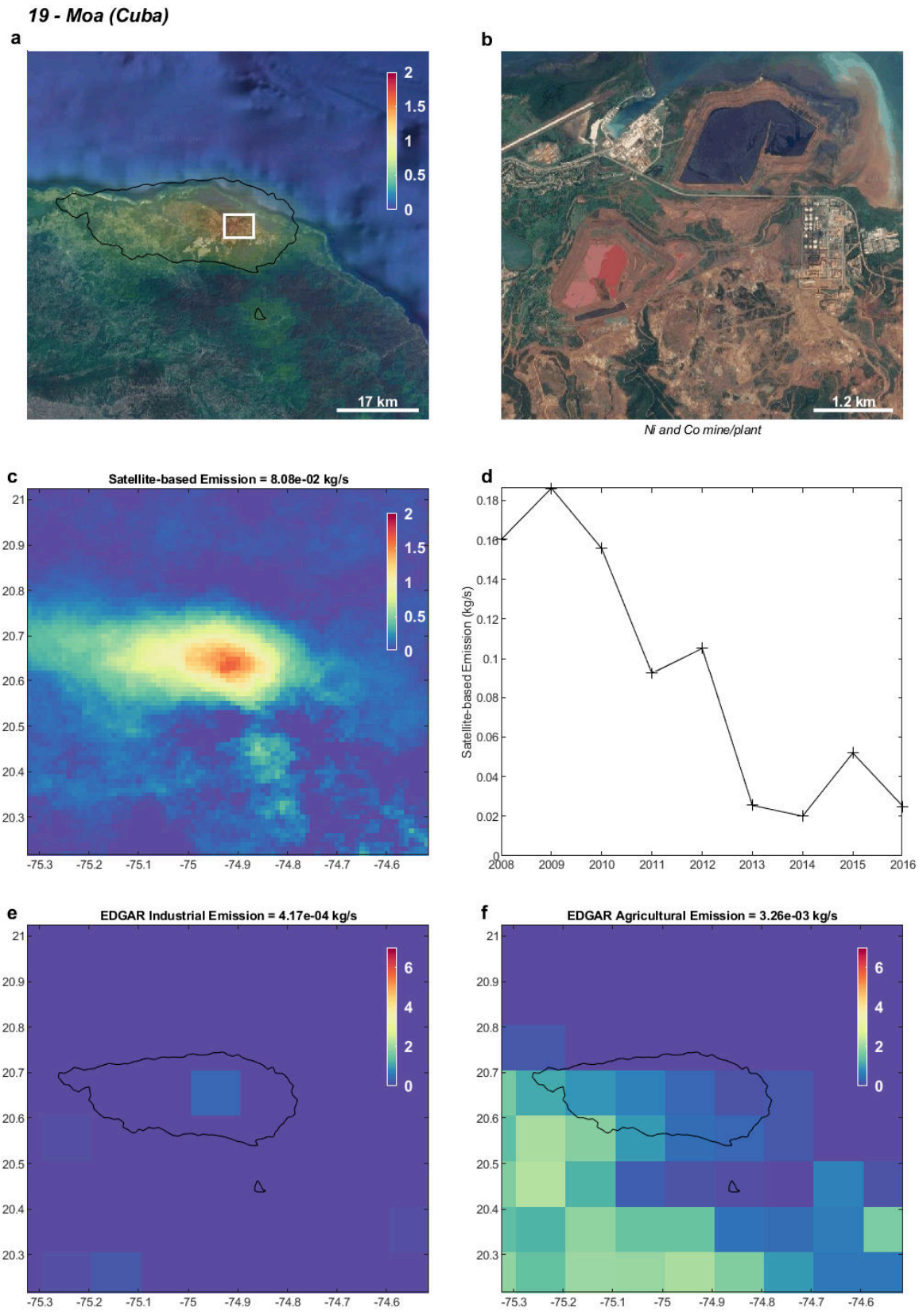

Historically, Cuba had three Cobalt-Nickel mines, one at Nicaro and two at Moa. Transport due to the dominant easterly winds can be observed, which also places the location of the hotspots slightly west of the likely emission sources. The Nicaro mine was closed in 2012, while production at one of Moa mines is currently reduced[1].

[1] https://www.havanatimes.org/?p=128296 (last access: 30/04/2018).

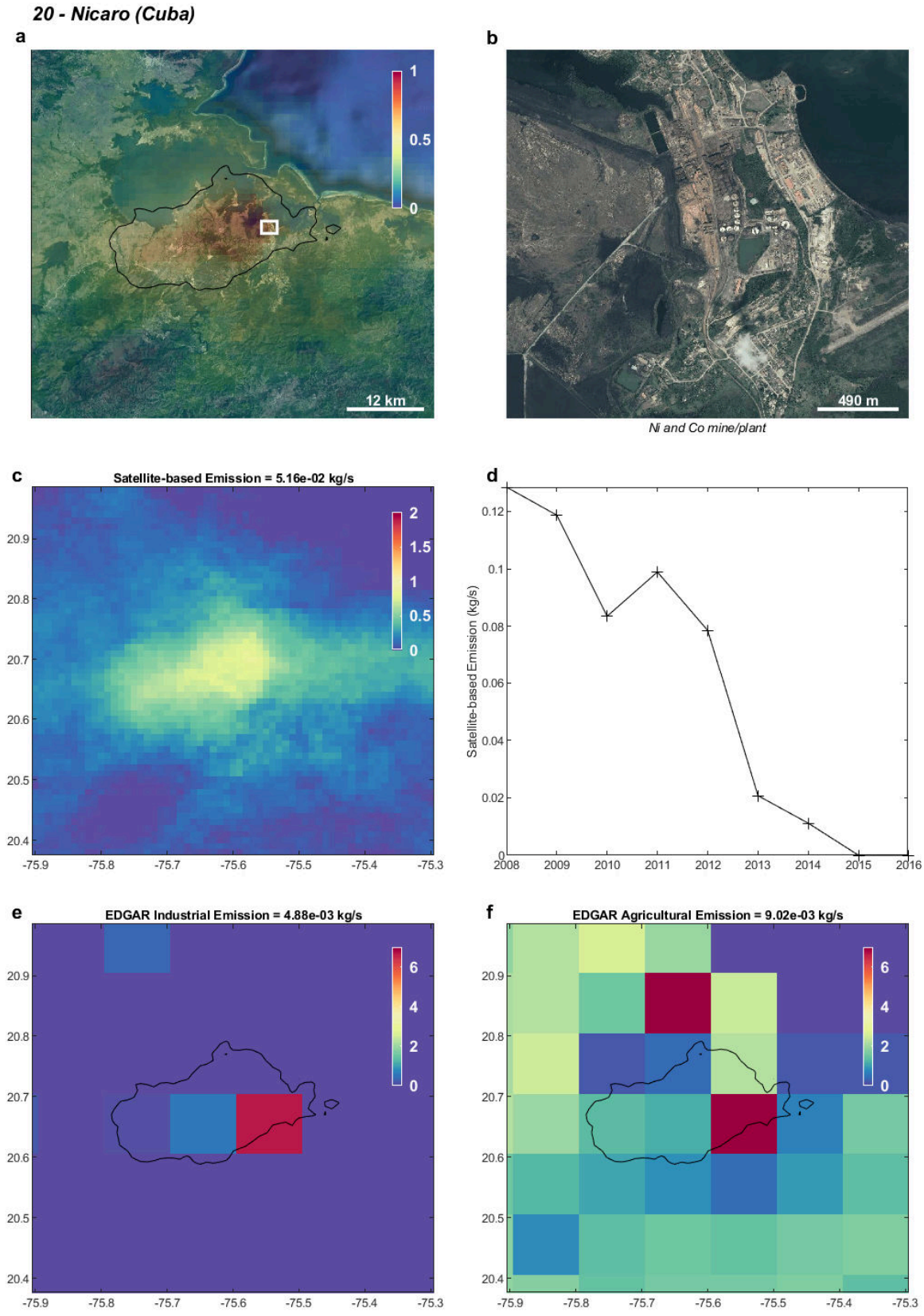

See previous.

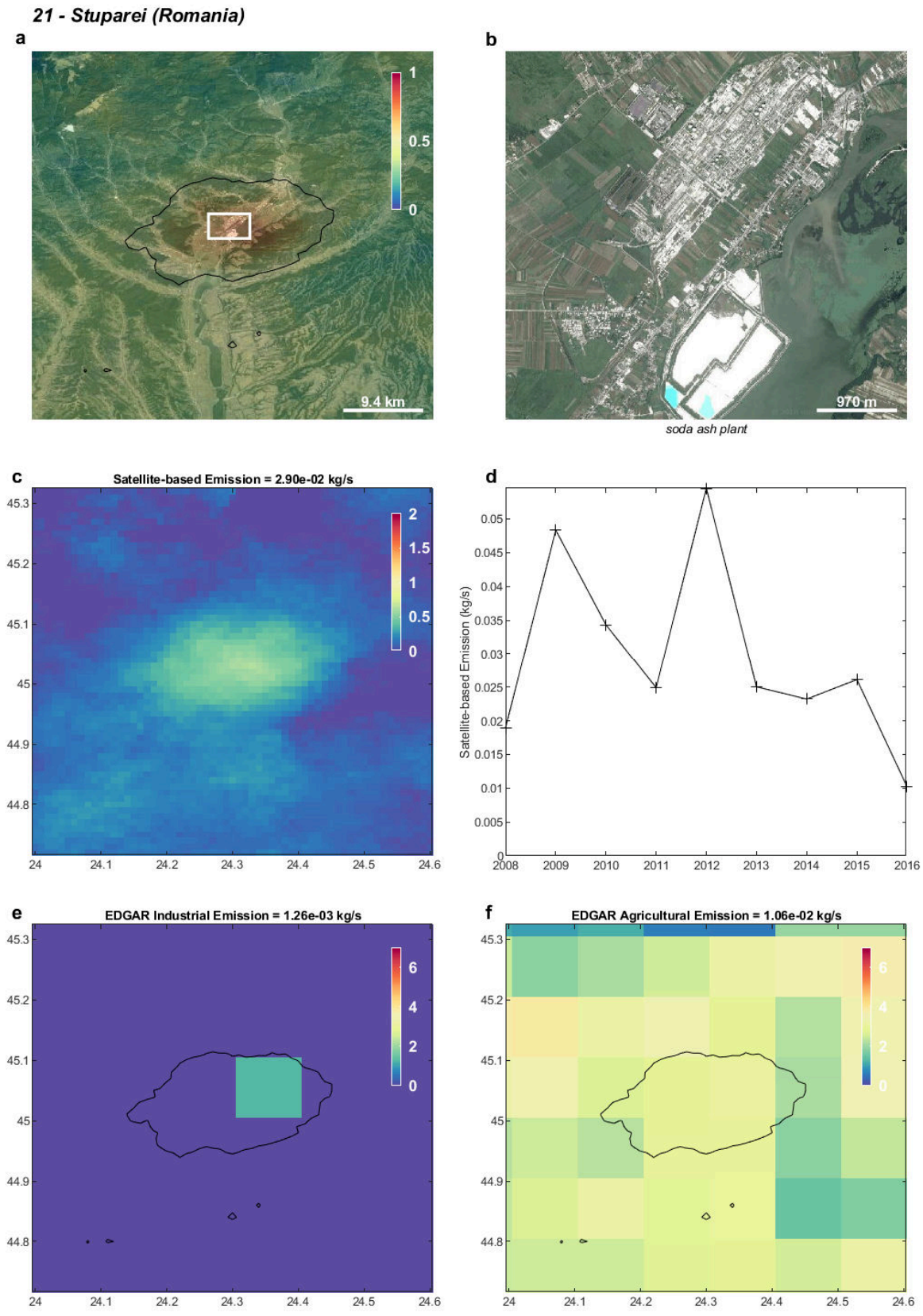

Near Stuparei lies a large soda ash factory and other sodium related industry. The industry relies on salt extracted from the mine in the nearby city of Ocnele Mari[1] and limestone from the nearby city of Arnota[2]. The observation of ammonia emissions over such a plant are not unexpected as NH_3 is used in the production of soda ash via the Solvay process (appropriately known as the ammonia-soda process)[3].

[1] Poenaru, V.D, Badea, A., Savin, E., Teleaga, D. & Poncos, V. Land degradation monitoring in the Ocnele Mari salt mining area using satellite imagery, Proc. SPIE 8181, Earth Resources and Environmental Remote Sensing/GIS Applications II, 81810U (27 October 2011); [2] Ploaie, G. & Turnock, D. Public perception of environment in the mountains of Vâlcea County. *GeoJournal* **55**, 683-701 (2001); [3] EMEP/EEA air pollutant emission inventory guidebook 2016, 2.B.7 Soda ash production (SNAP 040619) (2016).

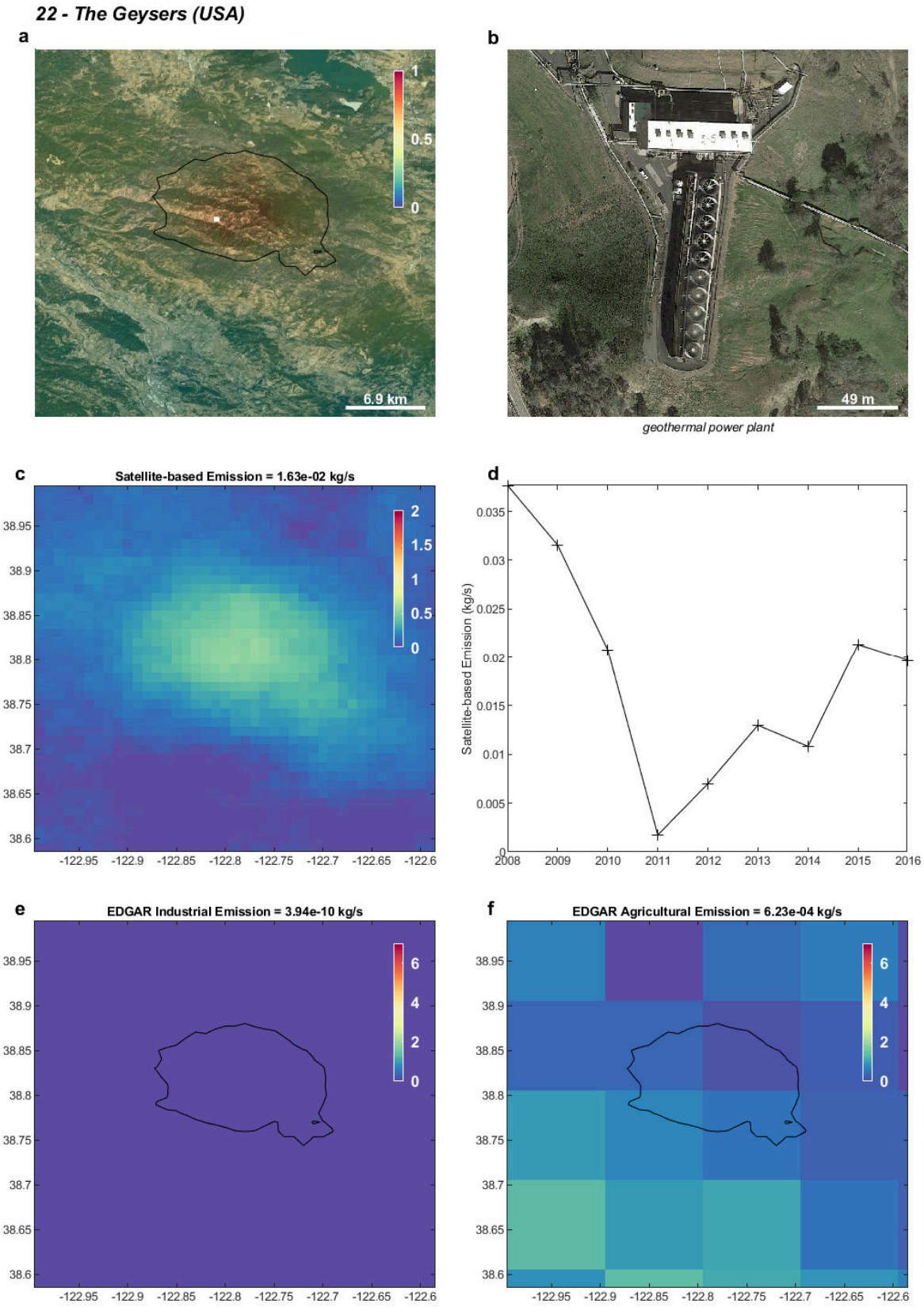

This complex of 22 plants makes up what is the largest geothermal power complex in the world. It is very likely the source of the observed NH_3 as the hotspot is located directly over the fields and as no other potential sources exist in this remote area. NH_3 is naturally present in geothermal steam, and may advantageously be used to neutralize co-emitted acidic sulphur species[1,2].

[1] Bravi, M. & Basosi, R. Environmental impact of electricity from selected geothermal power plants in Italy. *J. Cleaner Prod.* **66**, 301–308 (2014); [2] Boncian, R., Lenzi, A., Luperini, F. & Sabatelli, F. Geothermal power plants in Italy: increasing the environmental compliance, Conference: European Geothermal Congress 2013.

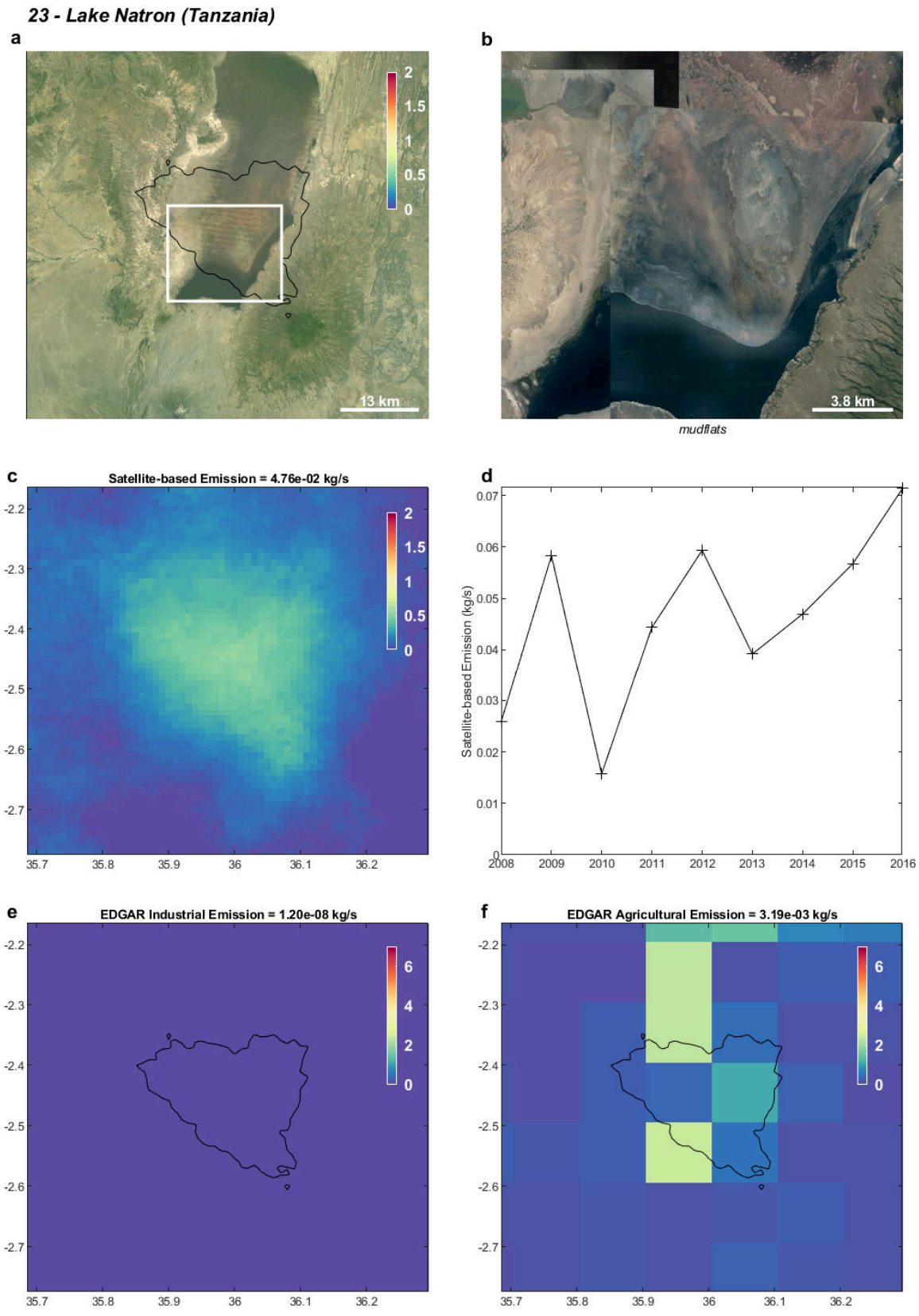

While there are a lot of different natural sources of NH_3, most of them are too diffuse to be observed as a hotspot. Lake Natron is a notable exception, it was classified to be of natural origin after having excluded anthropogenic sources (agriculture, industry, urban sources or fires) or retrieval artefacts. Decaying organic matter over Lake Natron's saline mudflats is thought to be the main source of the emissions observed here.

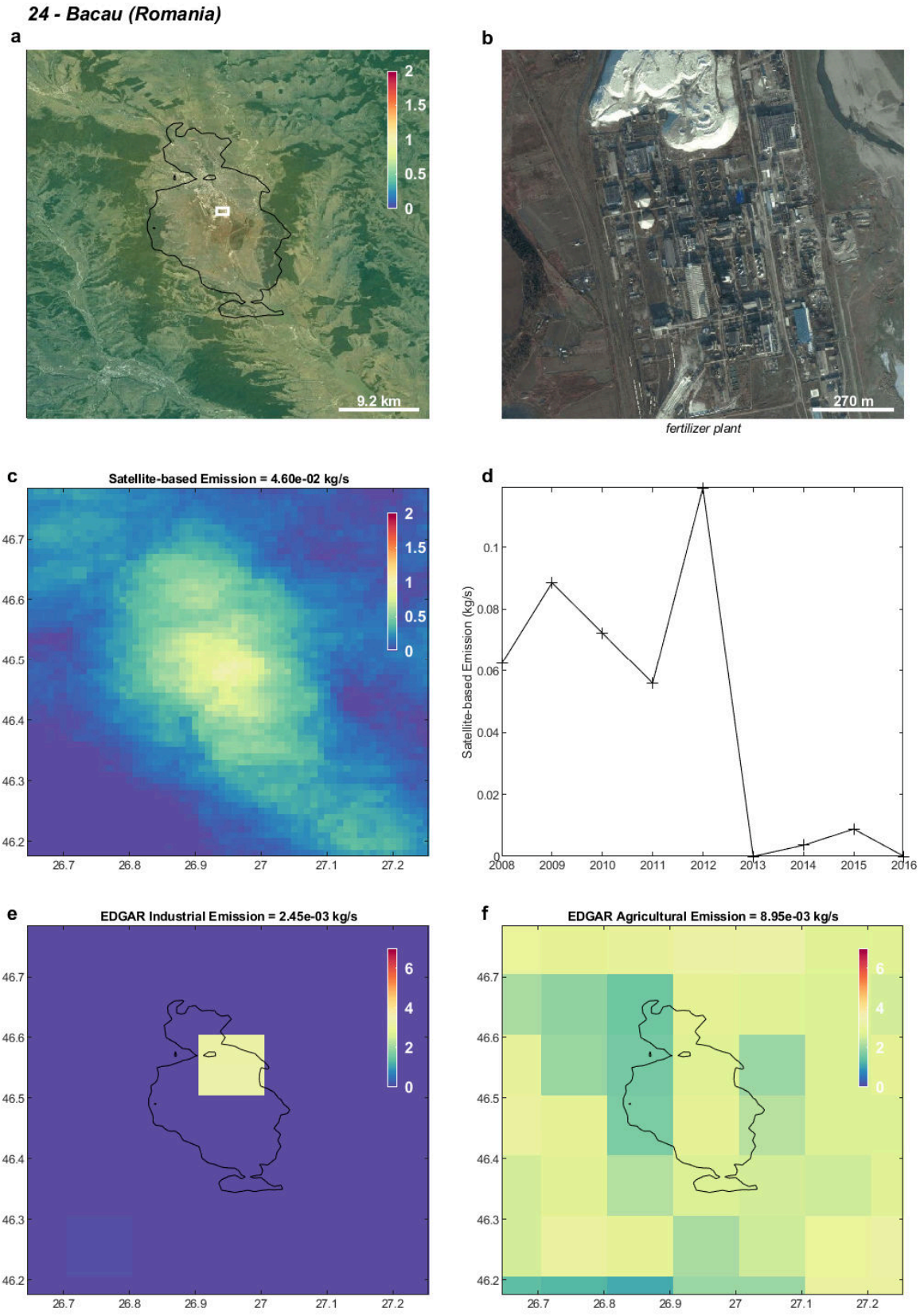

The NH_3 timeseries over this ammonia/urea plant in Bacau illustrates well how satellite measurements can be used to monitor temporal changes in NH_3 emissions. The sudden drop in 2013 likely corresponds to a production stop, following financial difficulties[1]. The site also made the news for casting the city of Bacau several times in a cloud of ammonia fog[2]. A large dump of phosphogypsum, a by-product in fertilizer production, can be seen north of the plant.

[1] http://www.economica.net/334-de-salariati-ai-combinatului-chimic-amurco-bacau-disponibilizati-colectiv-in-decembrie_67726.html (last access: 30/04/2018); [2] https://www.dcnews.ro/inca-o-amenda-luata-de-amurcao-bacau-pentru-poluare-cu-amoniac_126731.html (last access: 30/04/2018).

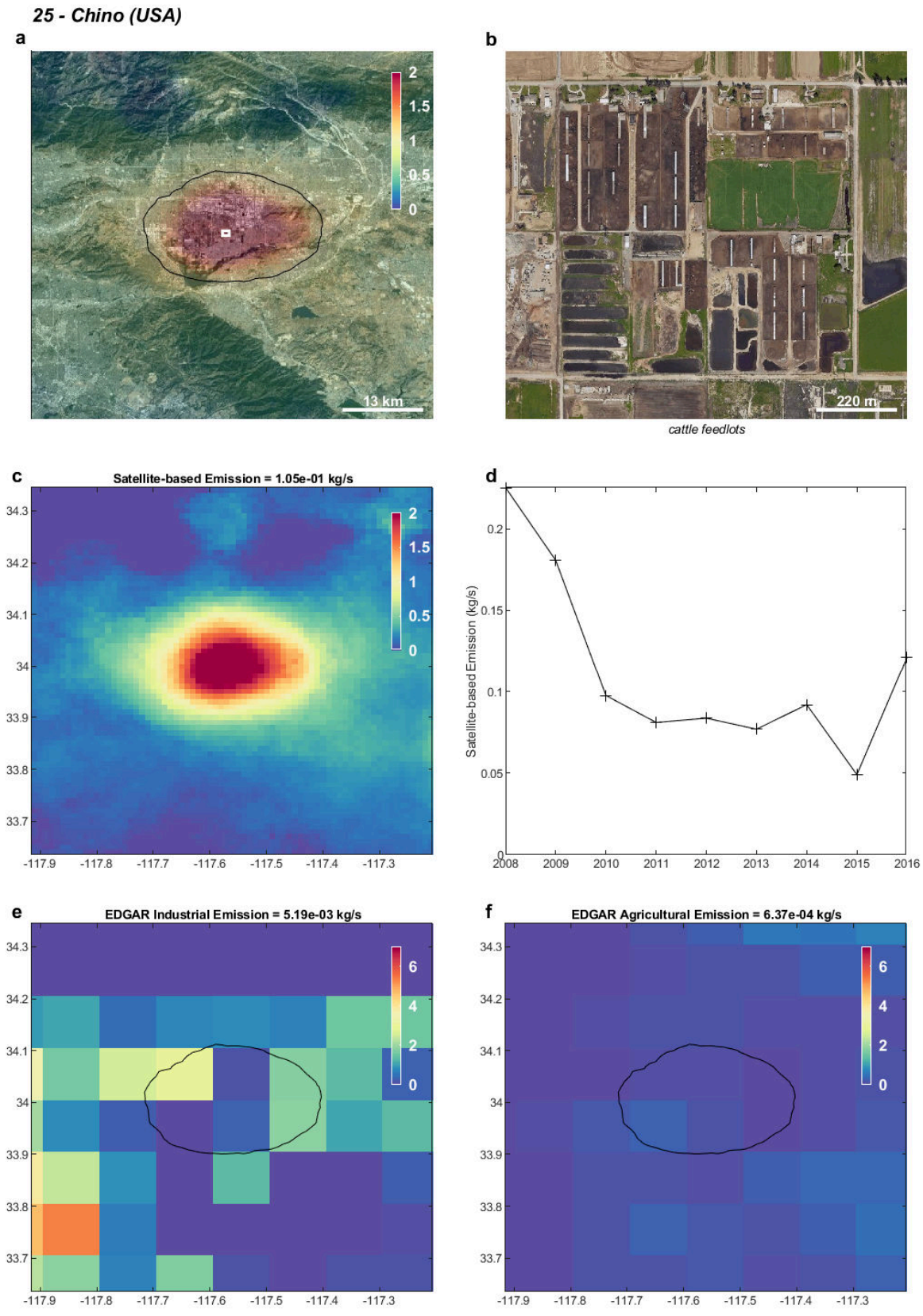

The Los Angeles Basin has since long been a stronghold for dairy farming. Due to urbanisation pressure these activities now take place in a few compact areas, namely Chino[1] (shown here) and Lakeview-San Jacinto (also a major NH_3 hotspot east of Chino).

[1] Leifer, I. *et al.* Remote sensing and in situ measurements of methane and ammonia emissions from a megacity dairy complex: Chino, CA. *Environ. Pollut*. **221**, 37-51 (2017).

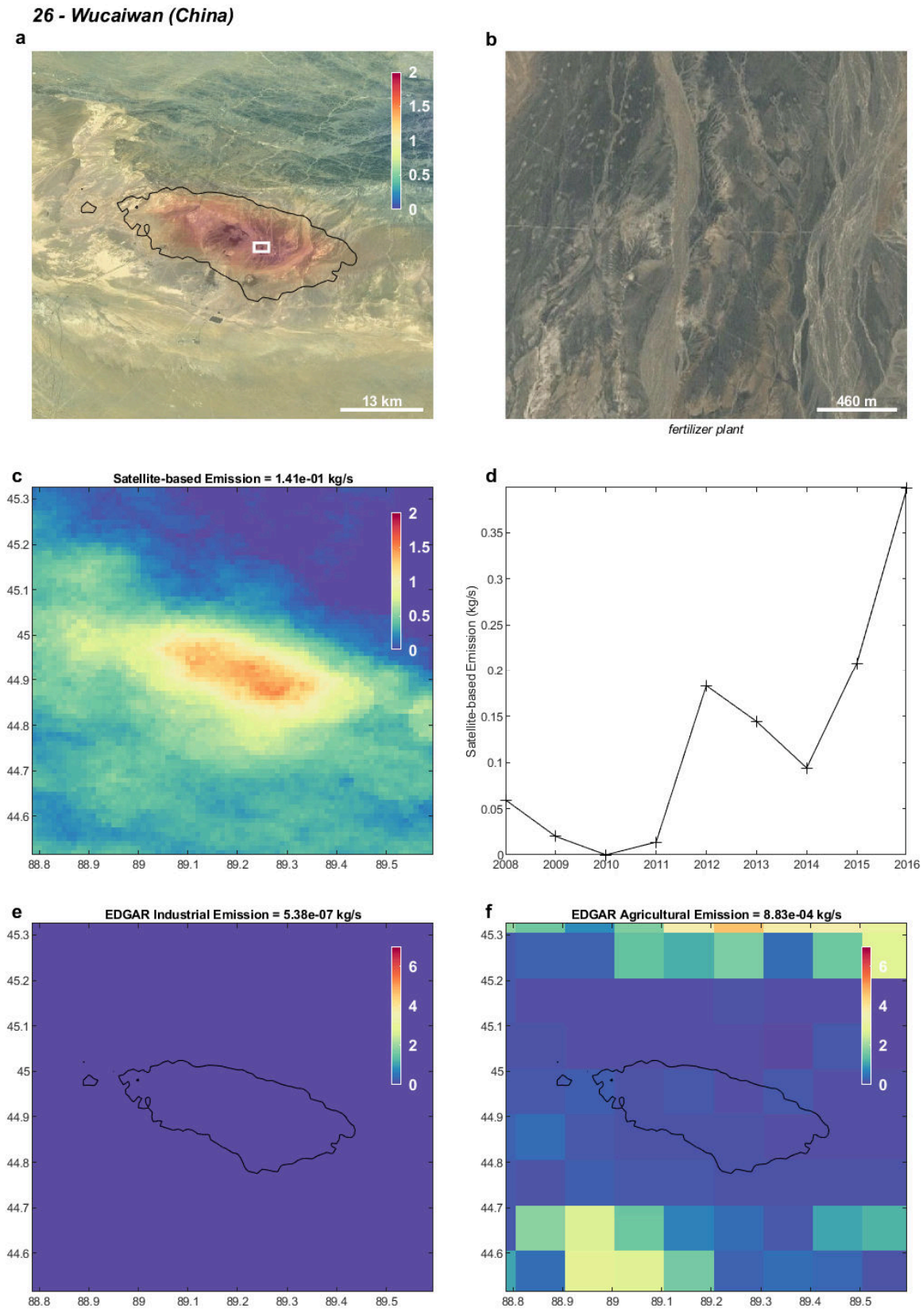

Located in the remote Dzungaria region of Xinjiang, the Wucaiwan region has extremely large reserves of coal. Located near a large coal-powered power plant, this ammonia and urea plant started production end of 2011[1].
See also Fig ED4 in the Extended Data section.

[1] http://www.fert.cn/news/2012/1/11/201211111551134573.shtml (last access: 30/04/2018).

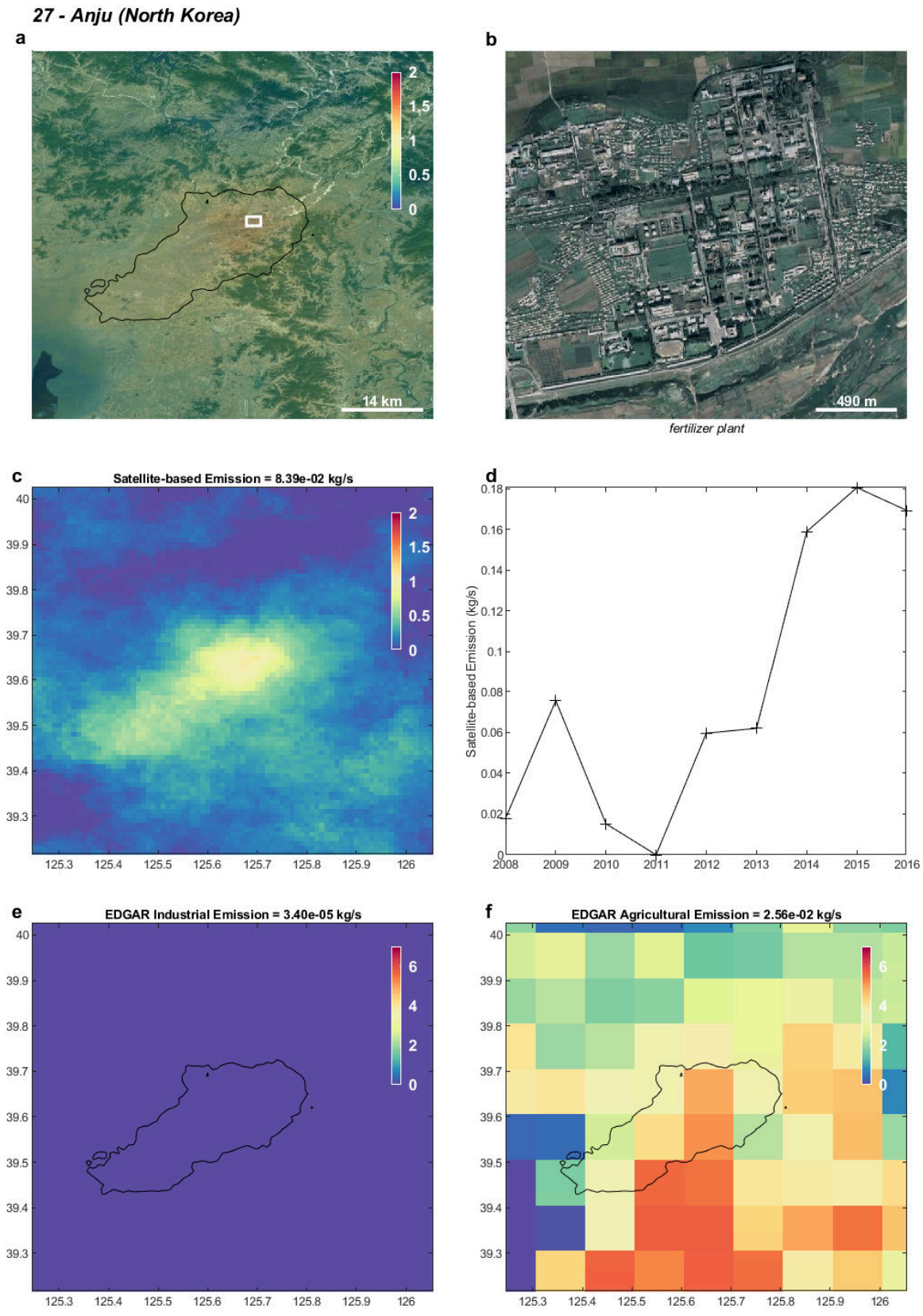

The Namhung Youth Chemical Complex near Anju was built in 1976 to produce, among other chemical products, ammonia and urea fertilizers. Renovation work started in 2008, which included the opening of two new gasification plants in 2010 and 2011[1].

[1] https://www.38north.org/2014/04/jbermudez041014/ (last access: 30/04/2018).

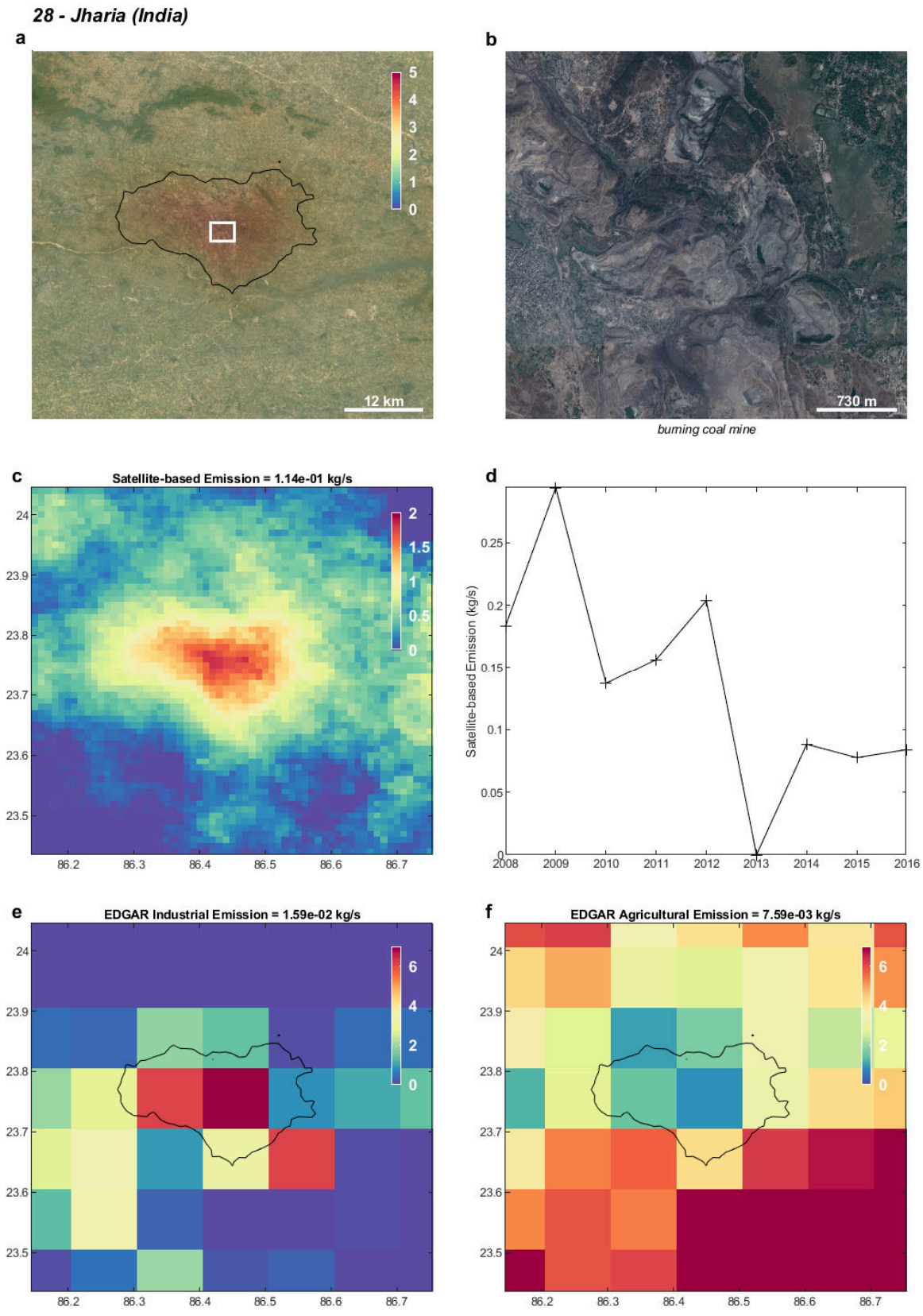

The NH_3 emission observed here are related to large scale underground fires in the coal mines of Jharia. These have been burning uncontrollably since 1916, as efforts to extinguish them have only partially been successful[1].

[1] Michalski, S. R. The Jharia mine fire control technical assistance project: an analysis. *Int. J. Coal Geol.* 59, 83-90 (2004).

B. Supplementary information related to NH_3 lifetime

Table SI1: NH_3 lifetime estimates reported in the literature.

REFERENCE	LIFETIME	COMMENT
Norman and Leck, 2005	Few hours	Clean remote ocean
	Several days	Dust/Biomass plumes over ocean
Quinn et al., 1990	Order of hours	Central Pacific Ocean
Flechard and Fowler, 1998	1-2 hours	Scottish moorland site
Sutton, 1990	10 hours	Using dry deposition velocity by Duyzer et al. (1987)
Möller and Schieferdecker 1985	19 hours	Using dry deposition rates of Mészáros and Horváth (1984)
Hertel et al., 2012	24 hours	Simulations over Europe
Dentener and Crutzen, 1994	Order of hours	
Whitburn et al., 2016	17-23 hours	Fire plume
Hauglustaine et al., 2014	15 hours	Average global model

References

- Dentener, F. J. & Crutzen, P. J. A three-dimensional model of the global ammonia cycle. *J. Atmos. Chem.* **19**, 331-369 (1994).
- Duyzer J. H., Bouman A. M. H., Diederen H. S. M. A. & Van Aalst R. M. Measurement of dry deposition velocities of NH_3 and NH_4^+ over natural terrains. Report R 87/273 Netherlands organisation for applied scientific research. MT-TNO, Delft, The Netherlands (1987).
- Flechard C., R. & Fowler, D. Atmospheric ammonia at a moorland site. I: The meteorological control of ambient ammonia concentrations and the influence of local sources. Quart. J. Roy. *Meteor. Soc.* **124**, 733-757 (1998).
- Hauglustaine, D. A., Balkanski, Y. & Schulz, M. A global model simulation of present and future nitrate aerosols and their direct radiative forcing of climate. *Atmos. Chem. Phys.* ***14***, 11031-11063 (2014).
- Hertel, O. *et al.* Governing processes for reactive nitrogen compounds in the European atmosphere. *Biogeosciences* **9**, 4921-4954 (2012).
- Mészáros E. & Horváth L. Concentration and dry deposition of atmospheric sulfur and nitrogen compounds under regional conditions in Hungary. *Atmos. Environ.* **18**, 1725-1730 (1984).
- Möller, D. & Schieferdecker, H. A relationship between agricultural NH_3 emissions and the atmospheric SO_2 content over industrial areas. *Atmos. Environ.* **19**, 695-700 (1985).
- Norman, M. & Leck, C. Distribution of marine boundary layer ammonia over the Atlantic and Indian Oceans during the Aerosols99 cruise. *J. Geophys. Res.-Atmos.* **110**, D16302 (2005).
- Quinn, P., Bates, T., Johnson, J., Covert, D. & Charlson, R. Interactions between the sulfur and reduced nitrogen cycles over the central Pacific Ocean. *J. Geophys. Res.-Atmos.* **95**, 16405-16416 (1990).
- Sutton, M. A. The surface/atmosphere exchange of ammonia. PhD Thesis, University of Edinburgh, 1990.
- Whitburn, S. *et al.* Doubling of annual ammonia emissions from the peat fires in Indonesia during the 2015 El Niño. *Geophys. Res. Lett.* **43**, 11,007–11,014 (2016).

C. Uncertainty analyses

Different factors contribute to the overall uncertainty in the satellite-based NH_3 emission estimates. As mentioned in the Methods section, and as demonstrated below, the uncertainty on the NH_3 lifetime represents the main uncertainty. A 12-hour mean effective lifetime has been used in this work, consistently with the few data available in the literature (see Table SI1). However, given the size of the boxes, and typical surface wind speeds, the effective lifetime is likely closer to a few hours for the smaller hotspots. The associated estimated emission fluxes are therefore likely larger than those estimated with a 12 hours lifetime. To provide robust lower and upper bounds, the emission fluxes were also calculated using conservative lower and upper bounds on the lifetime of 1 and 48 hours; the corresponding fluxes are shown as error bars in Figure 3.

Here we detail four uncertainty analyses that were carried out to quantify some of the smaller sources of uncertainty. In each case, a parameter associated to the retrieval or inversion was perturbed leading to alternative NH_3 concentrations or emission fluxes. Results of the analyses are summarized in Table SI2 and Figure SI4. The figure shows for each of the tests, a histogram of the differences in either concentration or emission fluxes between the baseline calculation (the one used in the paper) and the alternative calculation.

1. Data sampling

Because of the variable presence of clouds and the use of a filter that removes measurements with no information content (same dataset as in Van Damme et al., 2017) the temporal sampling in the oversampled average is not uniform. To assess to what extent the baseline sampling (that gives equal weight to each observation) affects the calculated fluxes, an alternative oversampled average was constructed where an equal weight was given to each month of the year. Practically this was constructed by averaging intermediary monthly averages. From there, the flux calculations were repeated and compared to the baseline fluxes reported in the paper. The histogram of the relative difference presented in Figure SI4 shows that the emission estimates differ by 4 % ± 7 %, i.e. the monthly-based averages are slightly lower. Note that the monthly-based average is not necessarily more correct as it is noisier due to the weight of months with fewer measurements (especially at higher latitudes).

2. Vertical profile

The IASI retrieval scheme that was used in this paper uses a fixed NH_3 vertical profile. To assess to what extent uncertainties on the vertical profile could introduce biases, we rely here on retrieval tests performed in Whitburn et al. (2016). In that paper, the baseline NH_3 retrieval that uses a fixed profile was compared with a retrieval that uses co-located variable GEOS-Chem simulated vertical profiles for the year 2009. Here we calculated the differences of all the measurements for that entire year to generate the statistics. As shown in the histogram (Figure SI4), differences are of the order of 2 % ± 24 %. These statistics are representative for the globe, but locally errors can be much larger. It should also be stressed that this analysis depends on the similarity of the fixed profile used in this study and the simulated GEOS-Chem vertical profiles, which may be substantially different from the actual vertical profiles.

3. Diurnal variability

To make a quantitative assessment of the importance of diurnal variability, model simulations from LOTOS-EUROS over Europe were used (same dataset as in Van Damme et al., 2014). This model explicitly takes into account the diurnal variability in the NH_3 emissions (Denier van der Gon et al., 2011). The fixed monthly and hourly temporal profiles considered for the simulations are presented in Van Damme et al. (2014). Figure SI2, left panel shows the columnar 2011 averages calculated from all hours of the day. The right panel illustrates the effect of sampling at the overpass time of IASI. Statistics of the entire year indicate the mean at the IASI overpass time is seen to be only slightly lower than the daily mean (4 % ± 8 % difference as shown in Figure SI4). Therefore, if the diurnal variability is realistically represented in LOTOS-EUROS, one can conclude that IASI

samples the mid-latitudes at a time that is more or less representative for the entire day. In reality, the diurnal cycle could differ significantly, so that the effect of the overpass time could be much larger than what emerges from this analysis.

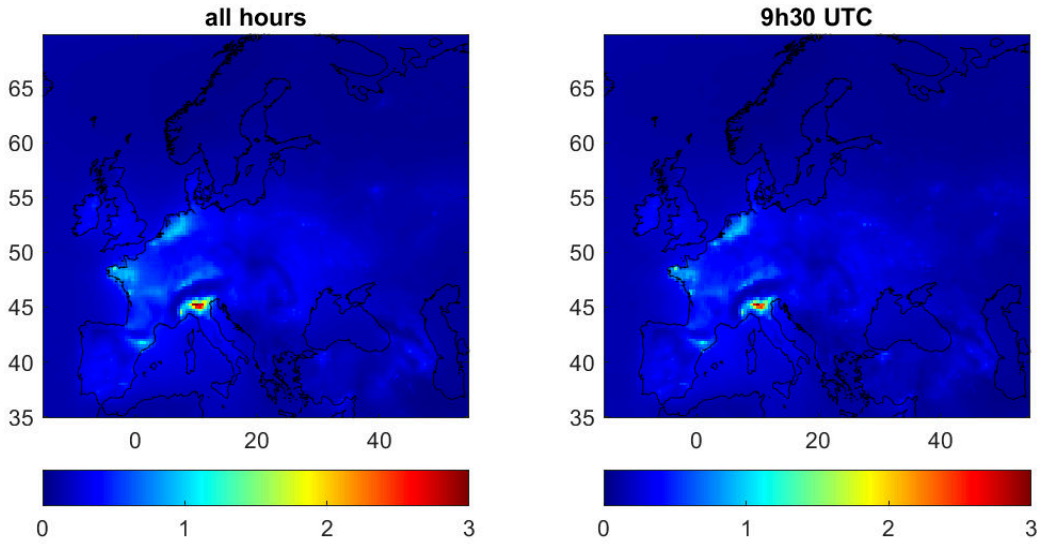

Figure SI2: Diurnal variability assessed with the LOTOS-EUROS model. (left) LOTOS-EUROS 2011 average NH_3 distribution (mg m^{-2}) using all hours of day and (right) using only the 9h30 UTC simulations.

4. Background correction

As detailed in the Methods section, for the flux calculations the background was determined as the percentile 10 value of all the pixels inside the box of each hotspot. To illustrate that this is a reasonable choice, we have tested alternative approaches. One alternative is to use the minimum value found inside the box as background. As illustrated in the Figure SI3 below with the example of Chino (California, USA), with this approach other background sources still contribute to the flux estimate calculation (see Figure SI3d). The background value could also be set to a larger value of the percentile. Figure SI3b illustrates what happens when the percentile 25 is used instead of the percentile 10. In this scenario, too much NH_3 is removed, resulting in large negative columns around the hotspot. Using the percentile 10, which gives a background correction somewhere in between these two extremes, is therefore deemed to be reasonable (Figure SI3c).

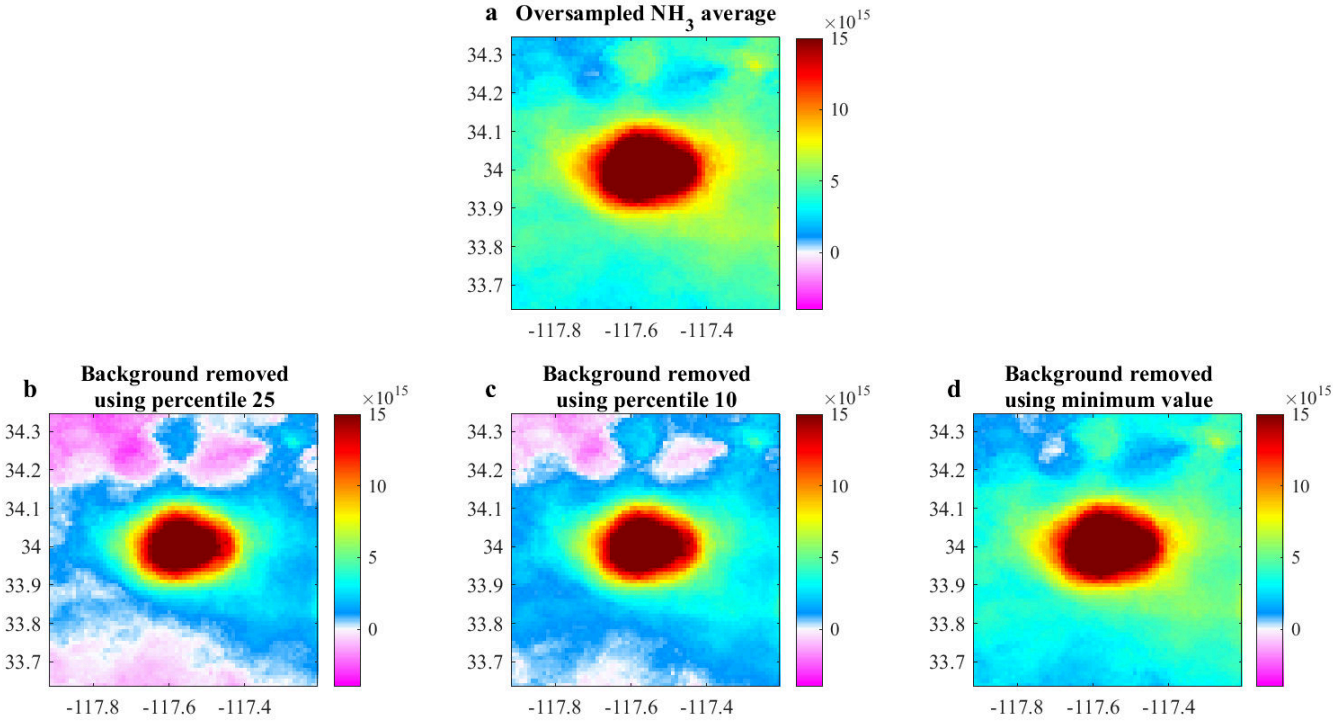

Figure SI3: Assessment of the background correction - distributions. (a) Nine-year average NH_3 hyperresolved map (molecules cm^{-2}) and resulting distributions (molecules cm^{-2}) obtained after subtracting the background calculated as the 25 percentile (b), the 10 percentile (c) and the minimum value (d).

To assess the order of magnitude of the error associated with the background correction, we have evaluated the impact on the fluxes for a background correction using the 5th and 15th percentile (two other reasonable alternatives) instead of the baseline 10th percentile. The results are again shown in Figure SI4, and point to differences of the order of - 18 / 14 % ± 7 / 5 %.

Table SI2: Summary of the uncertainty analysis. The biases refer to the relative differences (%) calculated as baseline data minus test data, divided by the baseline data. The uncertainties with respect to the seasonal sampling and background correction were calculated considering both regions and hotspots emission fluxes for the former and only the hotspots for the latter. The uncertainties with respect to the vertical profile and diurnal variabilities refer to NH_3 columns (global and over Europe respectively).

Uncertainty source	Bias	Standard deviation
Seasonal sampling	+ 4 %	7 %
Vertical Profile	+ 2 %	24 %
Background Correction	- 18 / 14 %	7 / 5 %
Diurnal variability	- 4 %	8 %

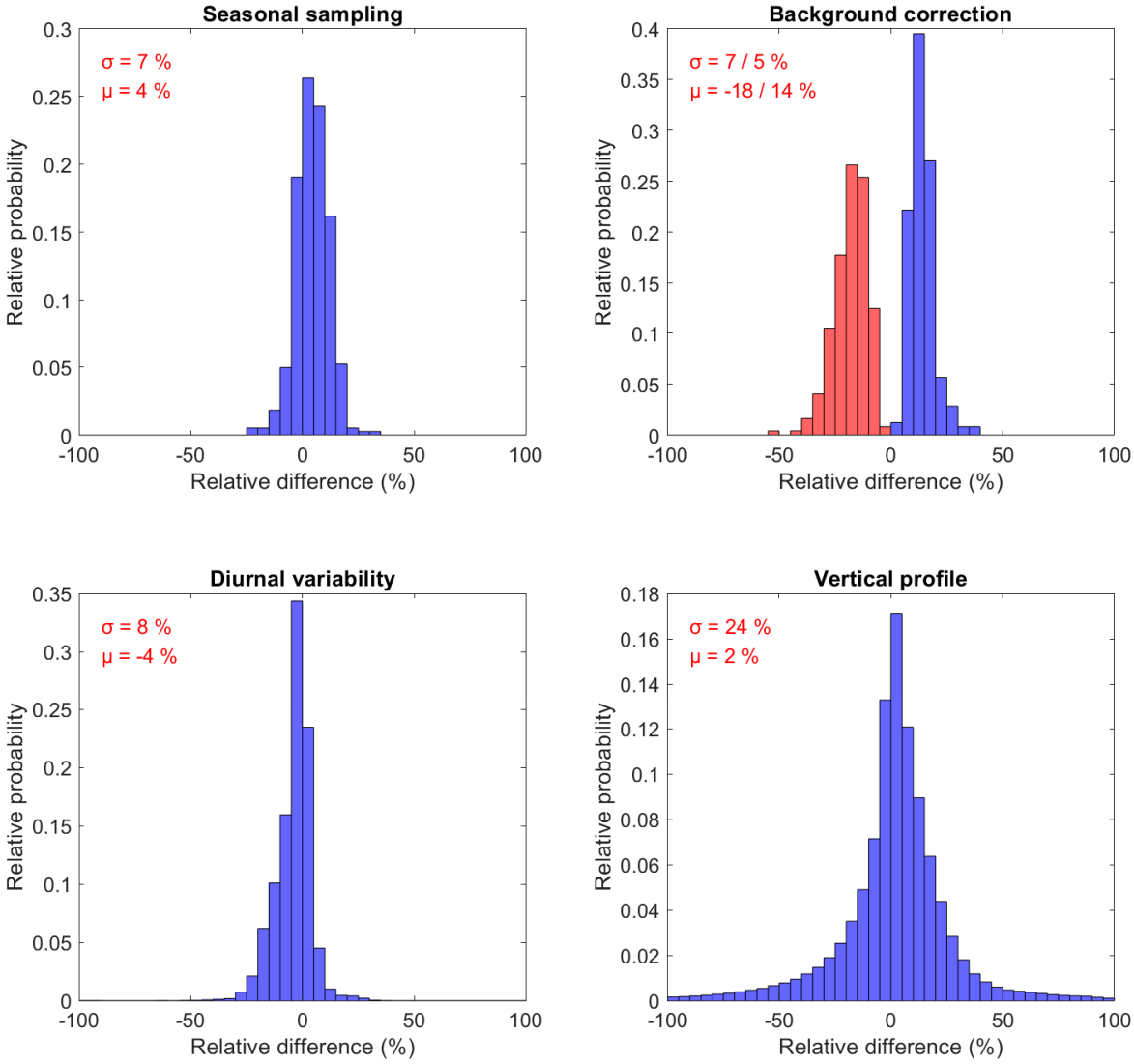

Figure SI4: Summary of the uncertainty analyses. The relative differences (%) are calculated as baseline data minus test data, divided by the baseline data. The uncertainties with respect to the seasonal sampling and background correction were calculated considering both regions and hotspots emission fluxes for the former and only the hotspots for the later. The uncertainties with respect to the vertical profile and diurnal variabilities refer to NH_3 columns (global and over Europe respectively).

References

- Denier van der Gon, H., Hendriks, C., Kuenen, J., Segers, A. & Visschedijk, A. Description of current temporal emission patterns and sensitivity of predicted AQ for temporal emission patterns, EU FP7 MACC Deliverable Rep. D_D-EMIS_1.3, TNO, Utrecht, The Netherlands (2011).
- Van Damme, M. *et al.* Evaluating four years of atmospheric ammonia (NH_3) over Europe using IASI satellite observations and LOTOS-EUROS model results. *J. Geophys. Res.-Atmos.* **119**, 9549-9566 (2014).
- Van Damme, M. *et al.* Version 2 of the IASI NH_3 neural network retrieval algorithm: near-real-time and reanalysed datasets. *Atmos. Meas. Tech.* **10**, 4905-4914 (2017).
- Whitburn, S. *et al.* A flexible and robust neural network IASI-NH_3 retrieval algorithm. *J. Geophys. Res.-Atmos.* **121**, 6581–6599 (2016).